Enhanced Linear Array Clustering via Hilbert Order

A. Benoni, P. Rocca, N. Anselmi, and A. Massa

2024/04/02

Contents

1 Numerical Results

In the following a set of numerical results will be reported.

1.1 Steered Pencil Beam Pattern, $N = 16$, $Q = 8$, $\theta_0 = -10$[deg]

In this first test case, let us apply the Hilbert Curve to sort the complex excitations of a linear phased array, and let us compare the obtained subarraying configuration with the best one achieved with the K-means approach. Different orders of Hilbert Curve have been evaluated.

Test Case Description

Antenna configuration

- isotropic elements

- number of elements: $N = 16$

- distance between elements along x axis: $d_x = \lambda/2$

Target excitations

- $w_n = \alpha_n e^{j\varphi_n}$ with $n = 1, .., N$

- main lobe steering: $\theta_0 = -10$ [deg]

- Taylor pattern

  - nominal sidelobe level: $SLL_{ref} = -30$ [dB]

  - polinomial order: $\bar{n} = 7$

Sub-array generation

- number of clusters: $Q = N/2 = 8$

- excitation matching strategies:

  - K-Means

  - Hilbert + BEM

1.1.1 K-Means Method

The best K-Means Method clusterized solution running the code $R = 50$ times is here reported.
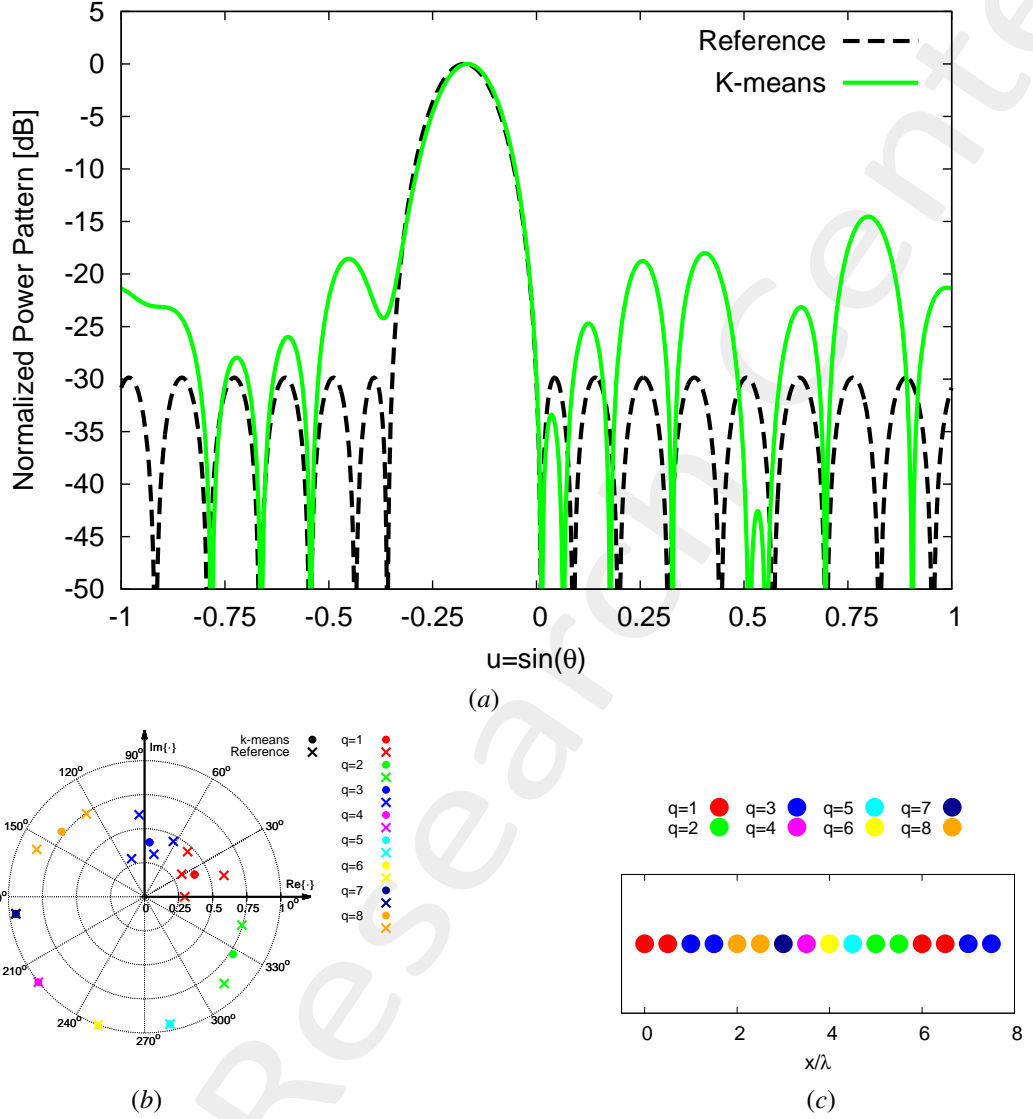

(a)

(b)

(c)

Figure 1: *Steered Pencil Beam* ($N = 16$, $Q = 8$, $\theta_0 = -10$ [deg]): plot of (*a*) the power pattern of the clusterized solutions together with the reference ones, (*b*) representation of the reference and the sub-array excitations in the complex plane, and (*c*) layout of the clustered array sytetized with the *KMM*.

Ψ^{opt}	Φ^{opt}	Γ^{opt}	SLL [dB]	D [dBi]	$\Delta\tau$ [sec]
2.73×10^{-2}	5.51×10^{-2}	1.68×10^{-1}	-14.53	11.24	0.109

Table I: *Steered Pencil Beam* ($N = 16$, $Q = 8$, $\theta_0 = -10$ [deg]): values of excitation matching index, Ψ^{opt}, the pattern matching index, Φ^{opt}, the pattern matching index Γ^{opt}, the SLL, the directivity D and the computational cost $\Delta\tau$.

1.1.2 Hilbert Curve Sorting + BEM

Different order of *Hilbert Curve* ($H = 1, .., 10$) have been here adopted to transform the 2D excitations space in a 1D space. The 1D Hilbert sorted excitations have been then clusterised according to the *Border Element Method* (BEM). $R = 50$ random initialization seeds have been tested and the best result in terms of excitation matching have been reported for each of the H Hilbert curve order.

Hilbert Curve Order: $H = 1$

Figure 2: *Steered Pencil Beam* ($N = 16$, $Q = 8$, $\theta_0 = -10$ [deg]): projection of the 2D complex target excitations along the Hilbert Curve of order $H = 1$.
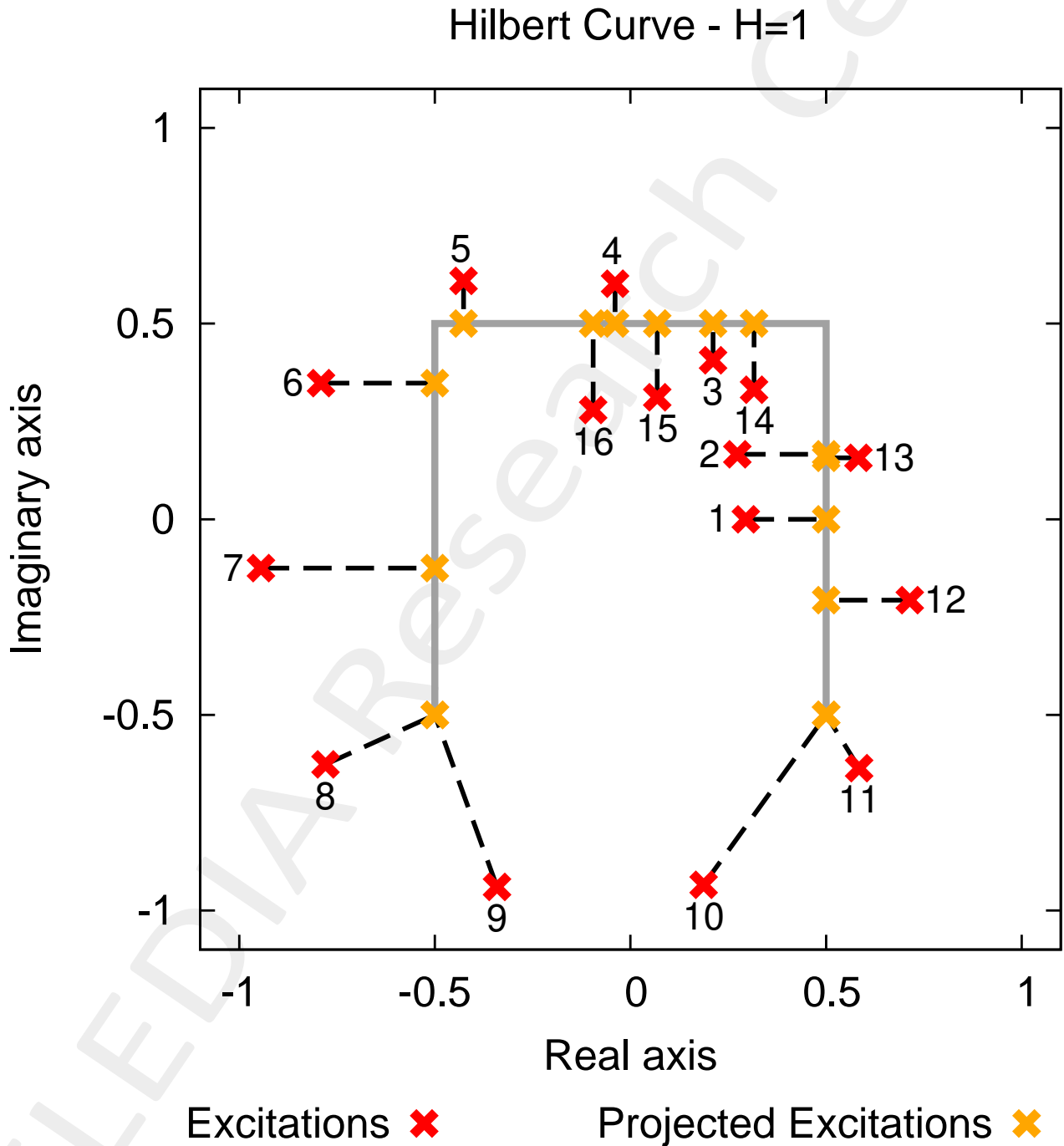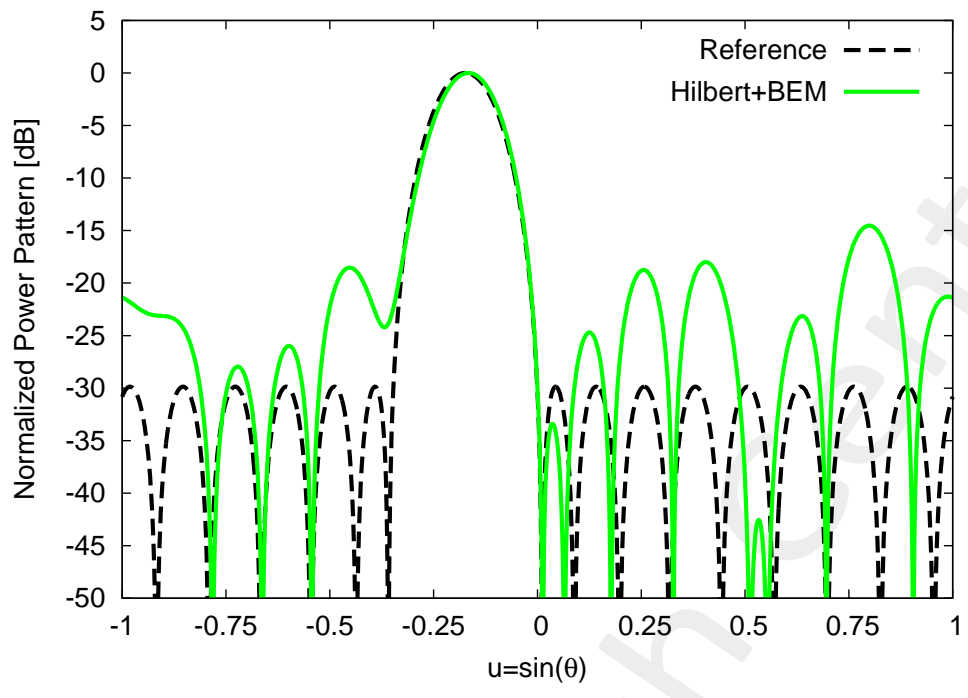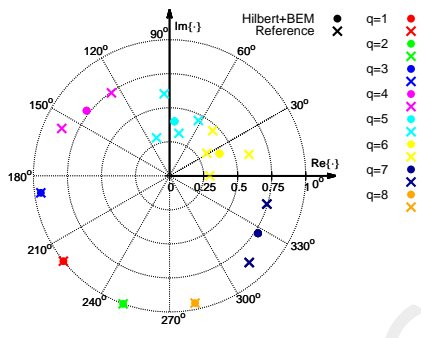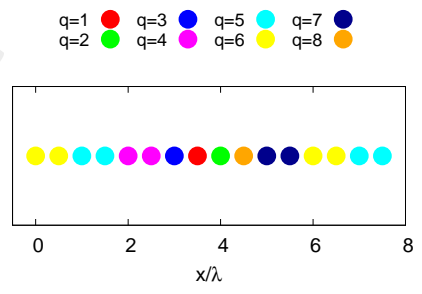
Figure 3: *Steered Pencil Beam* ($N = 16$, $Q = 8$, $\theta_0 = -10$ [deg]): plot of (*a*) the power pattern of the clusterized solutions together with the reference ones, (*b*) representation of the reference and the sub-array excitations in the complex plane, and (*c*) layout of the clustered array sythetized with *Hilbert+BEM,* obtained with the best seed.
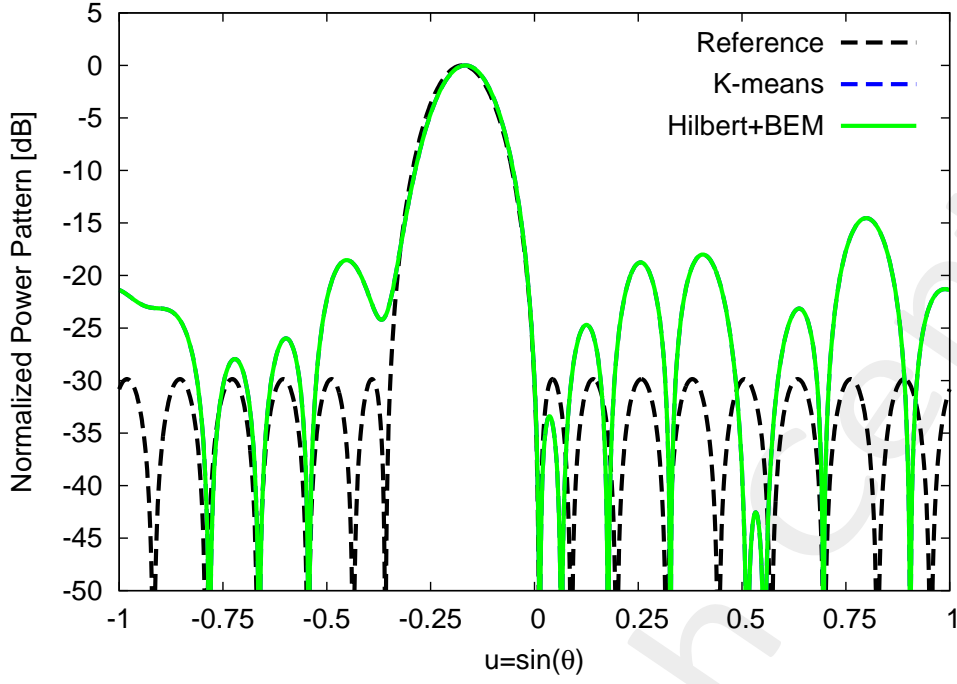
Figure 4: *Steered Pencil Beam* ($N = 16$, $Q = 8$, $\theta_0 = -10$ [deg]): power pattern of the clustered arrays synthetised with Hilbert+BEM, KMM together with the reference one.

Ψ^{opt}	Φ^{opt}	Γ^{opt}	SLL [dB]	D [dBi]	$\Delta\tau$ [sec]
2.73×10^{-2}	5.51×10^{-2}	1.68×10^{-1}	-14.53	11.24	2.37×10^{-3}

Table II: *Steered Pencil Beam* ($N = 16$, $Q = 8$, $\theta_0 = -10$ [deg]): values of excitation matching index, Ψ^{opt}, the field matching index, Φ^{opt}, the pattern matching index Γ^{opt}, the SLL, the directivity D and the computational cost $\Delta\tau$.

	min	max	μ	σ^2
Ψ^{opt}	2.73×10^{-2}	3.82×10^{-2}	3.36×10^{-2}	7.69×10^{-6}
Φ^{opt}	5.51×10^{-2}	7.83×10^{-2}	6.91×10^{-2}	3.30×10^{-5}
SLL [dB]	-16.93	-14.53	-15.33	0.26
D [dBi]	11.23	11.33	11.27	9.20×10^{-4}

Table III: Statistics (minimum value [min], maximum value [max], mean value [μ] and variance [σ^2]) calculated for the excitation matching Ψ^{opt}, the pattern matching index, Φ^{opt}, the SLL [dB] and the directivity D given $R = 50$ different random initialization.

Hilbert Curve - H=2

Figure 5: *Steered Pencil Beam* ($N = 16$, $Q = 8$, $\theta_0 = -10$ [deg]): projection of the 2D complex target excitations along the Hilbert Curve of order $H = 1$.

Figure 6: *Steered Pencil Beam* ($N = 16$, $Q = 8$, $\theta_0 = -10$ [deg]): plot of (*a*) the power pattern of the clusterized solutions together with the reference ones, (*b*) representation of the reference and the sub-array excitations in the complex plane, and (*c*) layout of the clustered array sythetized with *Hilbert+BEM,* obtained with the best seed.
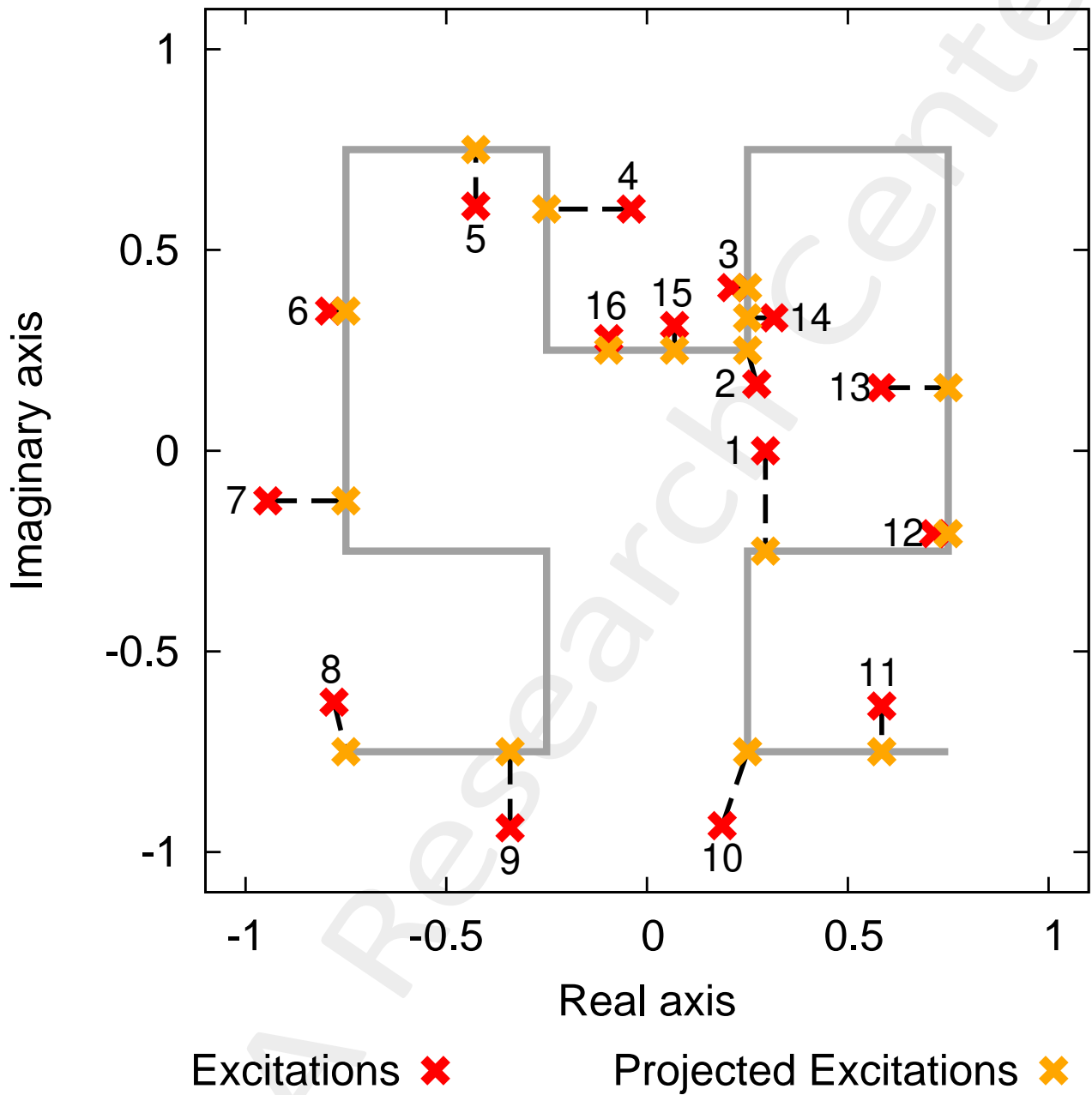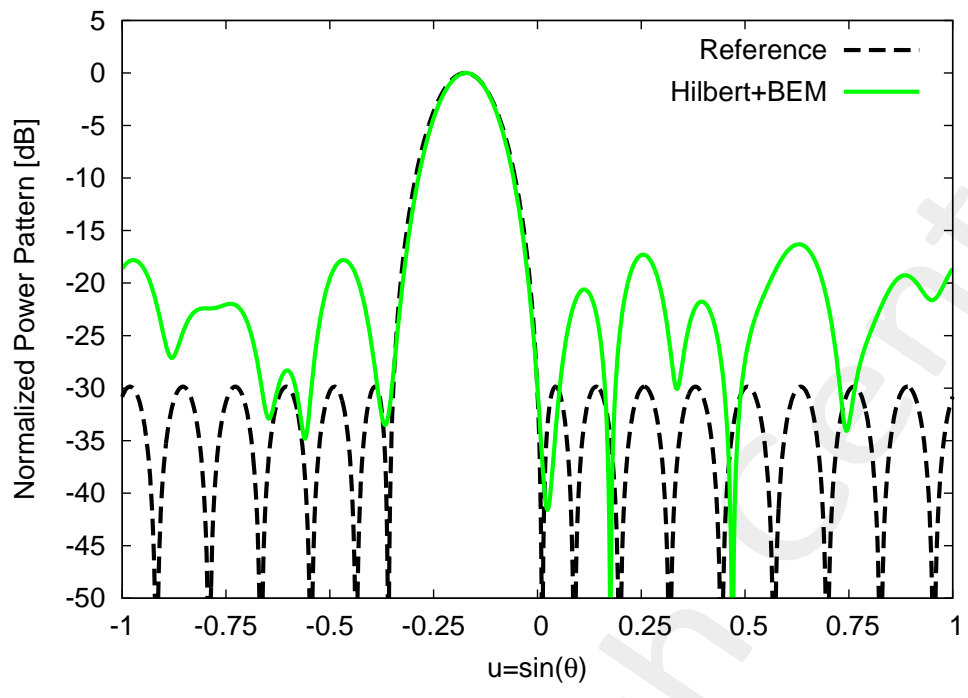
Figure 7: *Steered Pencil Beam* ($N = 16$, $Q = 8$, $\theta_0 = -10$ [deg]): power pattern of the clustered arrays synthetised with Hilbert+BEM, KMM together with the reference one.

Ψ^{opt}	Φ^{opt}	Γ^{opt}	SLL [dB]	D [dBi]	$\Delta\tau$ [sec]
3.10×10^{-2}	6.25×10^{-2}	1.92×10^{-1}	-16.30	11.30	2.53×10^{-3}

Table IV: *Steered Pencil Beam* ($N = 16$, $Q = 8$, $\theta_0 = -10$ [deg]): values of excitation matching index, Ψ^{opt}, the pattern matching index, Φ^{opt}, the pattern matching index Γ^{opt}, the SLL, the directivity D and the computational cost $\Delta\tau$.

	min	max	μ	σ^2
Ψ^{opt}	3.10×10^{-2}	6.50×10^{-2}	3.98×10^{-2}	1.19×10^{-4}
Φ^{opt}	6.25×10^{-2}	1.32×10^{-1}	8.16×10^{-2}	4.84×10^{-4}
SLL [dB]	-16.30	-13.79	-15.15	0.44
D [dBi]	11.01	11.30	11.22	8.20×10^{-3}

Table V: Statistics (minimum value [min], maximum value [max], mean value [μ] and variance [σ^2]) calculated for the excitation matching Ψ^{opt}, the pattern matching index, Φ^{opt}, the SLL [dB] and the directivity D given $R = 50$ different random initialization.
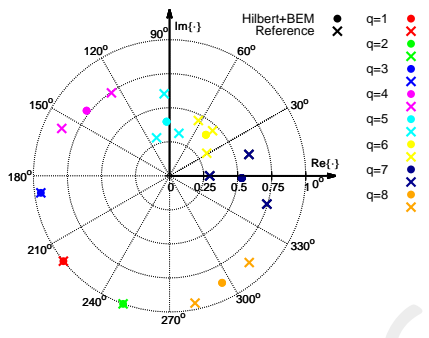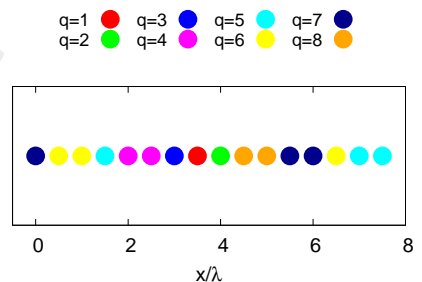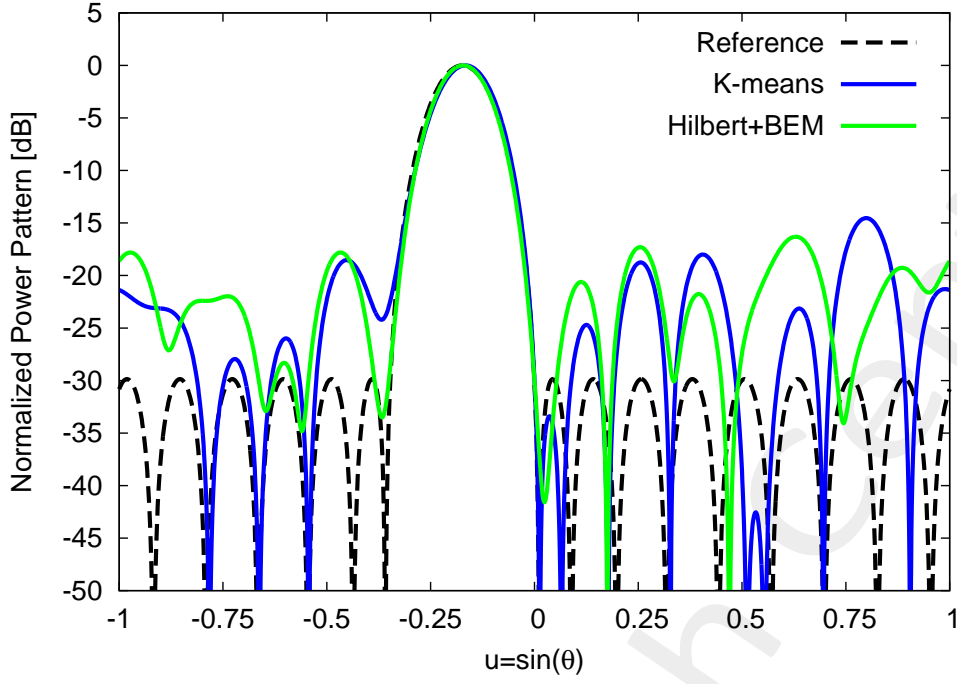
Figure 8: *Steered Pencil Beam* ($N = 16$, $Q = 8$, $\theta_0 = -10$ [deg]): projection of the 2D complex target excitations along the Hilbert Curve of order $H = 3$.

Figure 9: *Steered Pencil Beam* ($N = 16$, $Q = 8$, $\theta_0 = -10$ [deg]): plot of (*a*) the power pattern of the clusterized solutions together with the reference ones, (*b*) representation of the reference and the sub-array excitations in the complex plane, and (*c*) layout of the clustered array sythetized with *Hilbert+BEM*, obtained with the best seed.
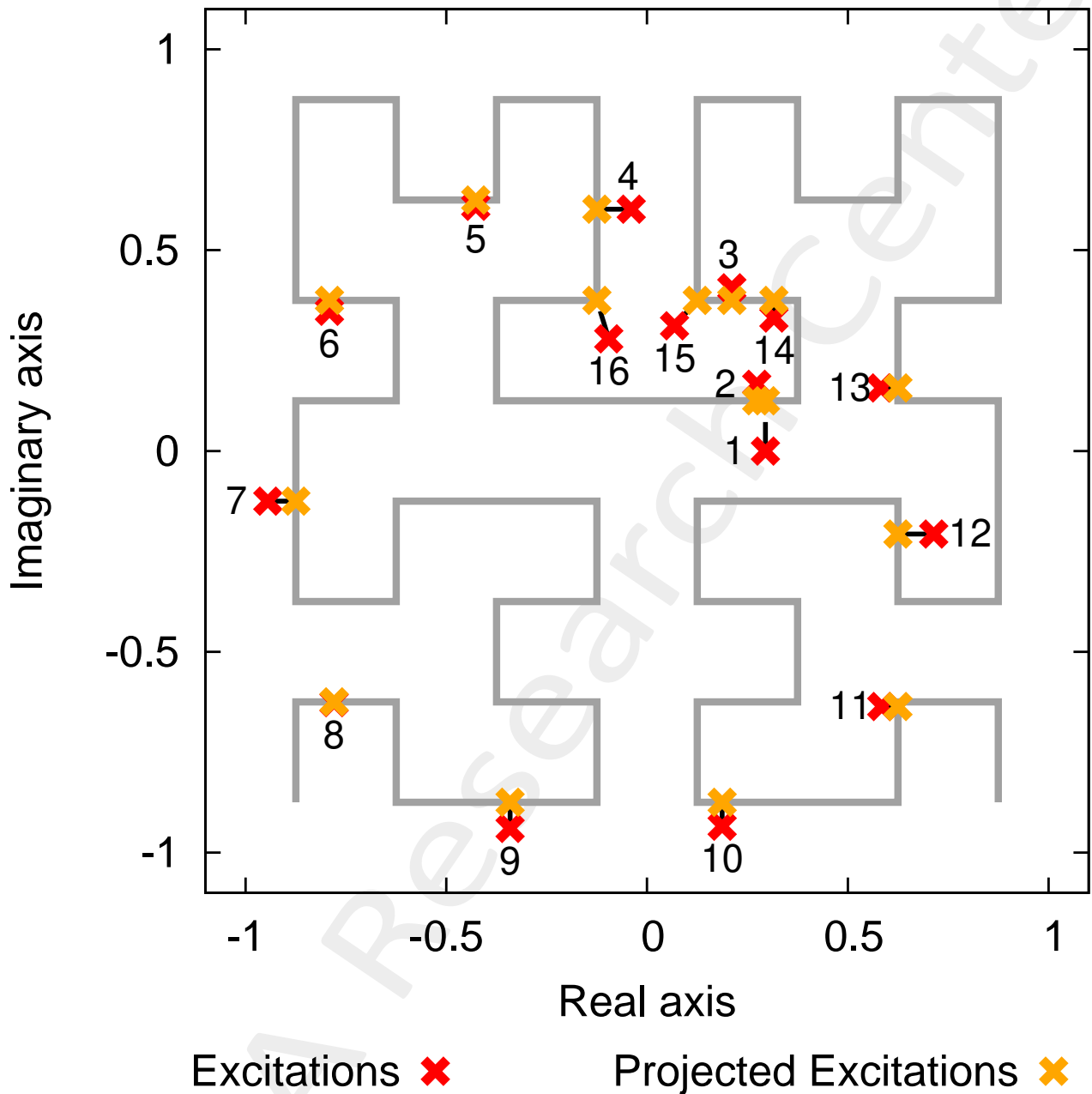
Figure 10: *Steered Pencil Beam* ($N = 16$, $Q = 8$, $\theta_0 = -10$ [deg]): power pattern of the clustered arrays synthetised with Hilbert+BEM, KMM together with the reference one.

Ψ^{opt}	Φ^{opt}	Γ^{opt}	SLL [dB]	D [dBi]	$\Delta\tau$ [sec]
3.10×10^{-2}	6.26×10^{-2}	2.04×10^{-1}	-16.41	11.15	2.80×10^{-3}

Table VI: *Steered Pencil Beam* ($N = 16$, $Q = 8$, $\theta_0 = -10$ [deg]): values of excitation matching index, Ψ^{opt}, the pattern matching index, Φ^{opt}, the pattern matching index Γ^{opt}, the SLL, the directivity D and the computational cost $\Delta\tau$.

	min	max	μ	σ^2
Ψ^{opt}	3.10×10^{-2}	5.58×10^{-2}	3.89×10^{-2}	4.66×10^{-5}
Φ^{opt}	6.26×10^{-2}	1.14×10^{-1}	7.97×10^{-2}	1.88×10^{-4}
SLL [dB]	-16.53	-12.43	-14.60	1.23
D [dBi]	10.89	11.24	11.16	7.19×10^{-3}

Table VII: Statistics (minimum value [min], maximum value [max], mean value [μ] and variance [σ^2]) calculated for the excitation matching Ψ^{opt}, the pattern matching index, Φ^{opt}, the SLL [dB] and the directivity D [dBi] given $R = 50$ different random initialization.
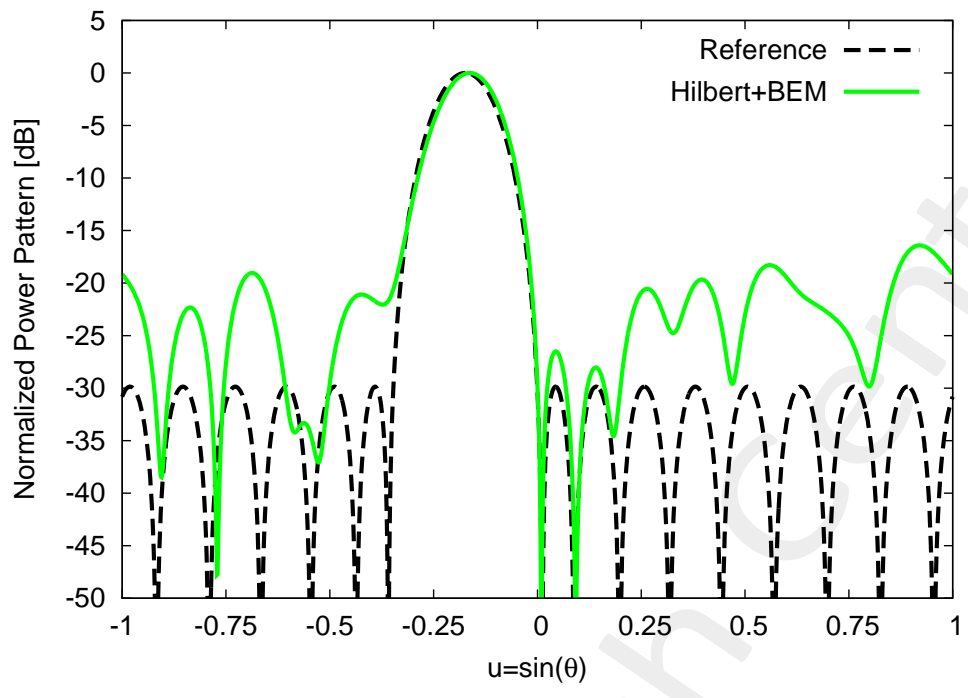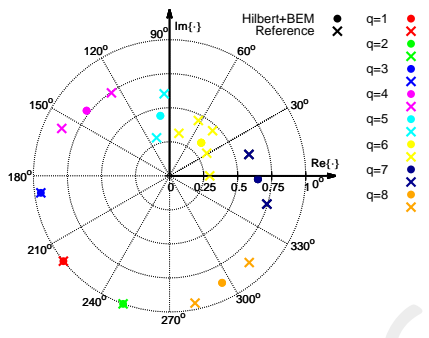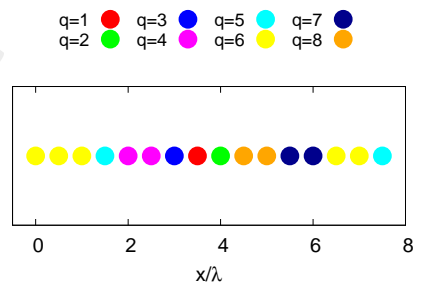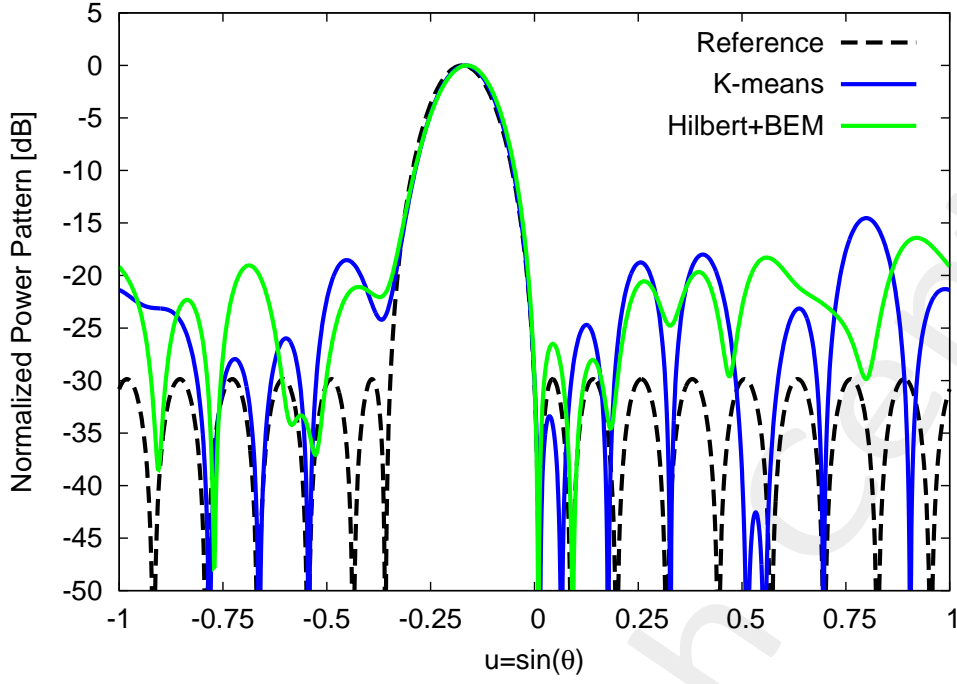
Figure 11: *Steered Pencil Beam* ($N = 16$, $Q = 8$, $\theta_0 = -10$ [deg]): projection of the 2D complex target excitations along the Hilbert Curve of order $H = 1$.

Figure 12: *Steered Pencil Beam* ($N = 16$, $Q = 8$, $\theta_0 = -10$ [deg]): plot of (*a*) the power pattern of the clusterized solutions together with the reference ones, (*b*) representation of the reference and the sub-array excitations in the complex plane, and (*c*) layout of the clustered array sytetized with *Hilbert+BEM,* obtained with the best seed.
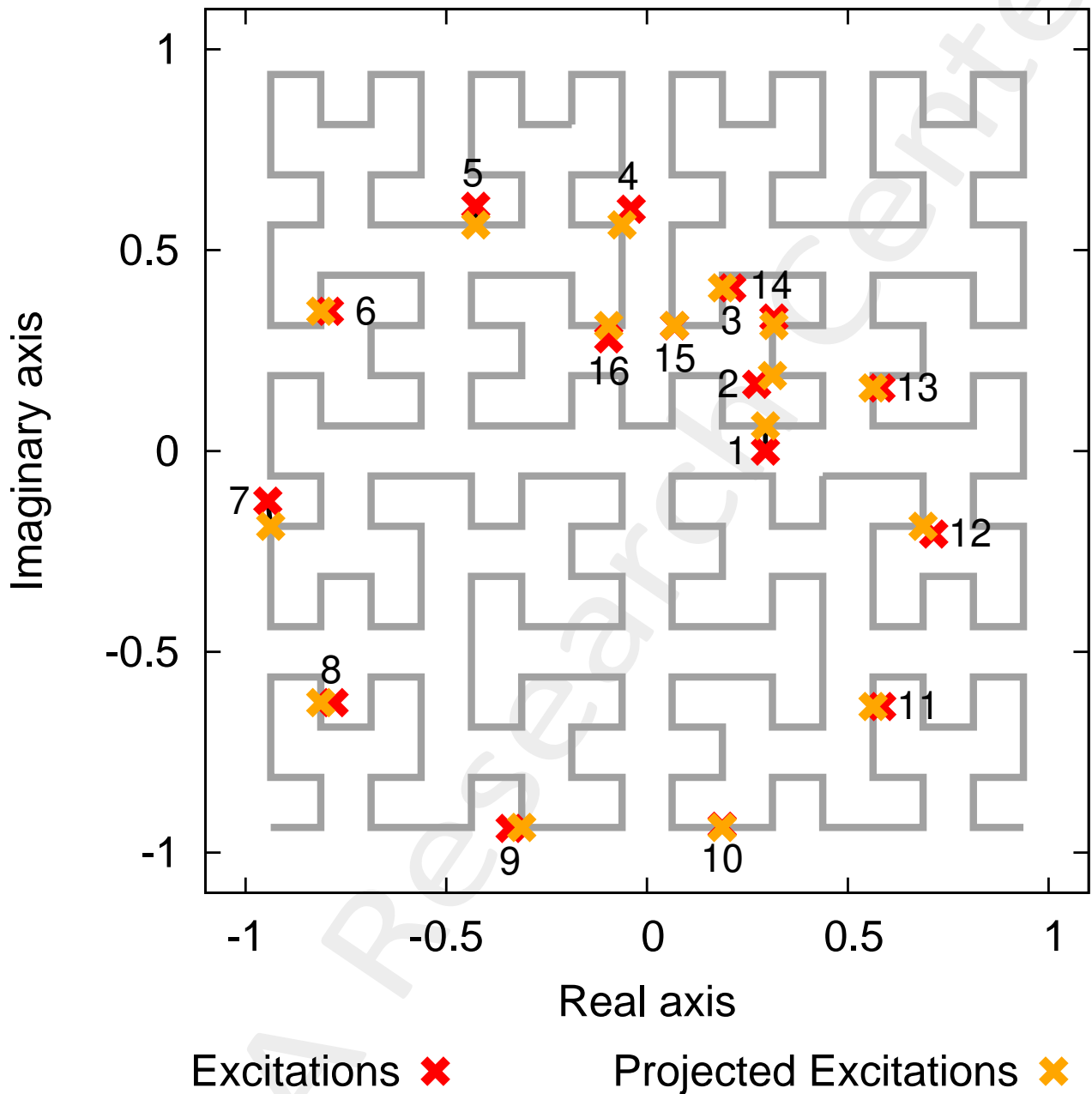
Figure 13: *Steered Pencil Beam* ($N = 16$, $Q = 8$, $\theta_0 = -10$ [deg]): power pattern of the clustered arrays synthetised with Hilbert+BEM, KMM together with the reference one.

Ψ^{opt}	Φ^{opt}	Γ^{opt}	SLL [dB]	D [dBi]	$\Delta\tau$ [sec]
3.24×10^{-2}	6.67×10^{-2}	1.87×10^{-1}	-15.78	11.15	2.90×10^{-3}

Table VIII: *Steered Pencil Beam* ($N = 16$, $Q = 8$, $\theta_0 = -10$ [deg]): values of excitation matching index, Ψ^{opt}, the pattern matching index, Φ^{opt}, the pattern matching index Γ^{opt}, the SLL, the directivity D and the computational cost $\Delta\tau$.

	min	max	μ	σ^2
Ψ^{opt}	3.24×10^{-2}	5.58×10^{-2}	3.84×10^{-2}	3.74×10^{-5}
Φ^{opt}	6.67×10^{-2}	1.14×10^{-1}	7.88×10^{-2}	1.50×10^{-4}
SLL [dB]	-16.53	-12.43	-14.28	1.16
D [dBi]	10.95	11.24	11.17	6.04×10^{-3}

Table IX: Statistics (minimum value [min], maximum value [max], mean value [μ] and variance [σ^2]) calculated for the excitation matching Ψ^{opt}, the pattern matching index, Φ^{opt}, the SLL [dB] and the directivity D [dBi] given $R = 50$ different random initialization.
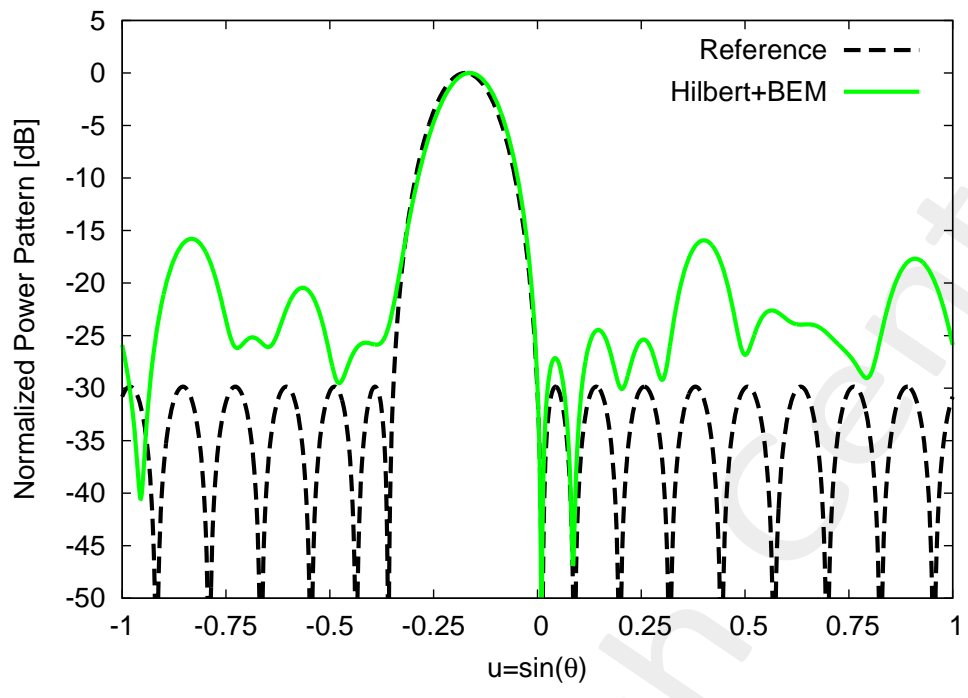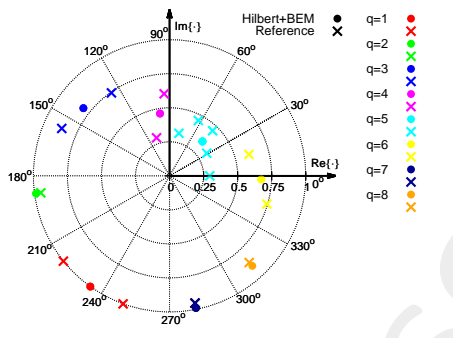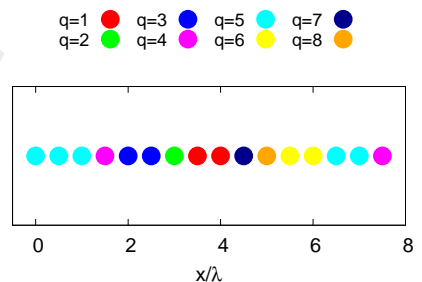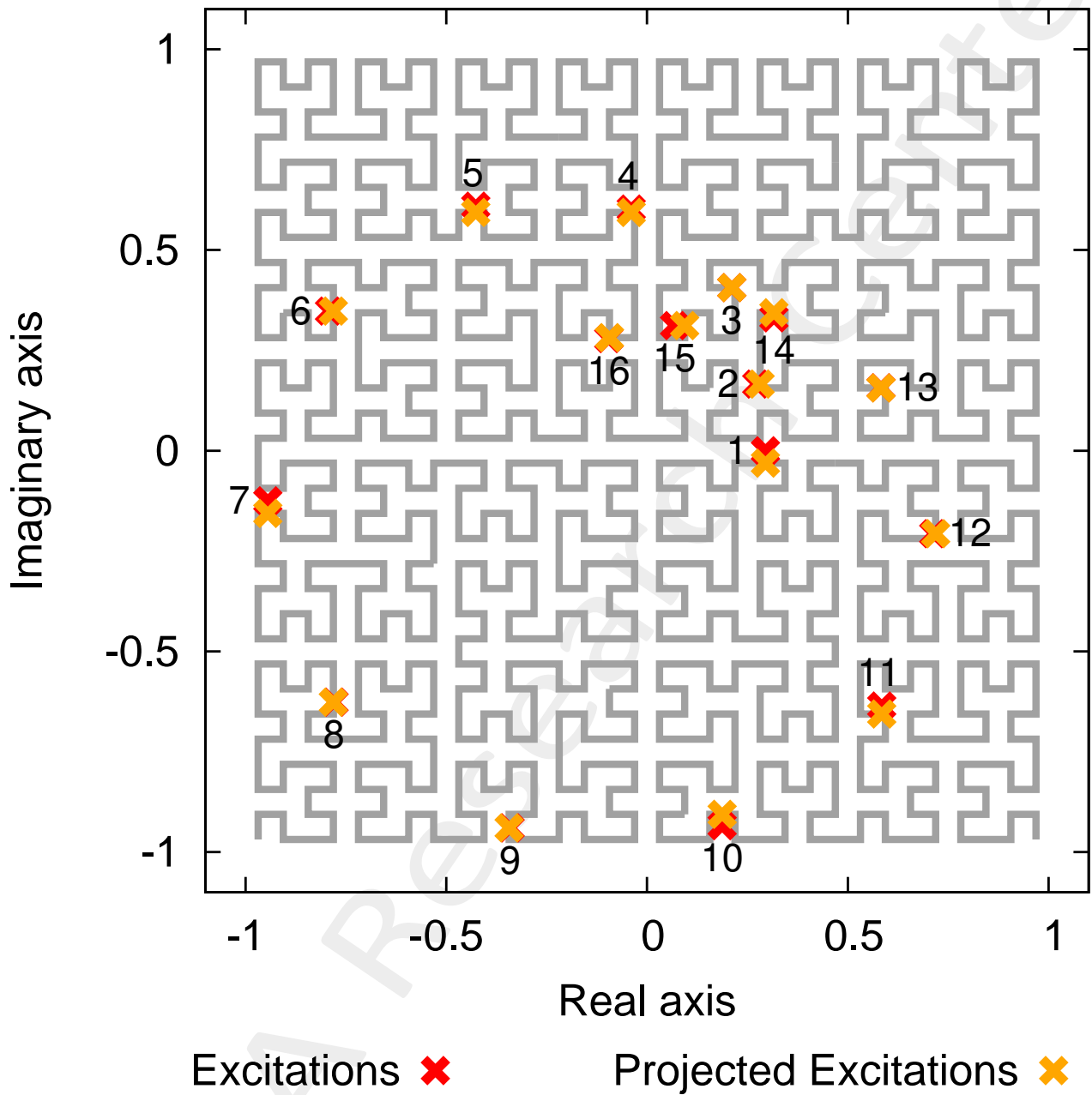
Figure 14: *Steered Pencil Beam* ($N = 16$, $Q = 8$, $\theta_0 = -10$ [deg]): projection of the 2D complex target excitations along the Hilbert Curve of order $H = 1$.
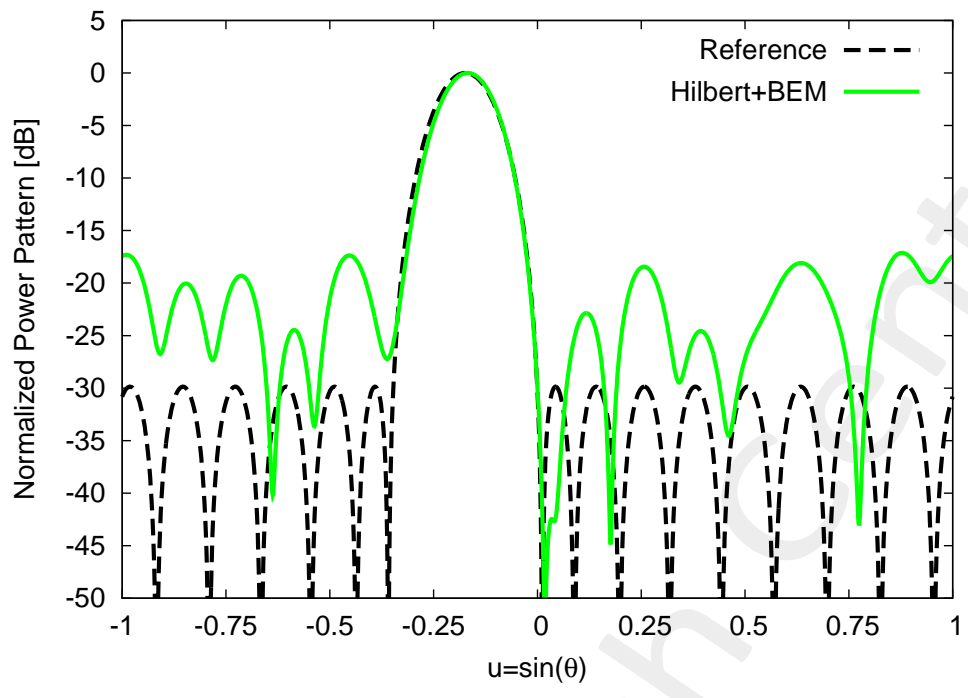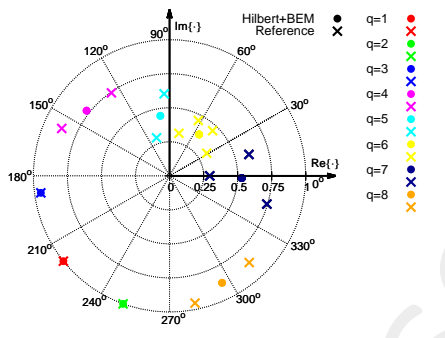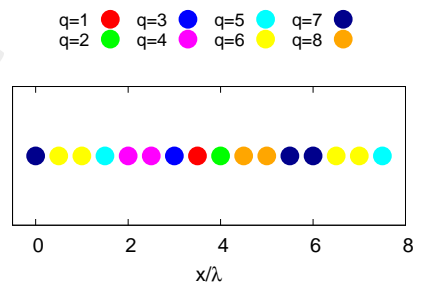
Figure 15: *Steered Pencil Beam* ($N = 16$, $Q = 8$, $\theta_0 = -10$ [deg]): plot of (*a*) the power pattern of the clusterized solutions together with the reference ones, (*b*) representation of the reference and the sub-array excitations in the complex plane, and (*c*) layout of the clustered array sythetized with *Hilbert+BEM*, obtained with the best seed.
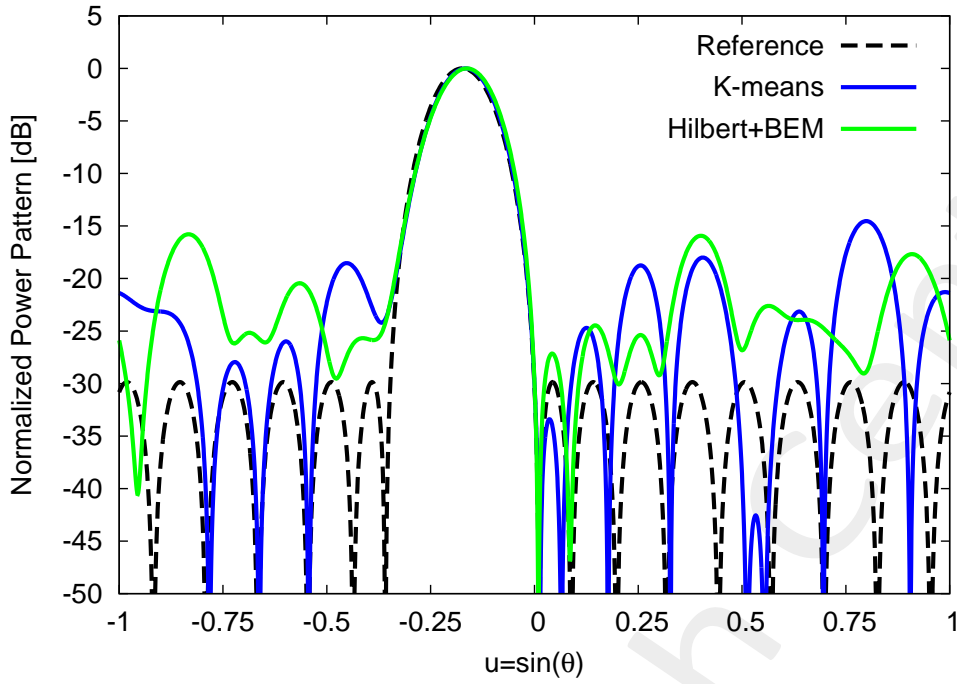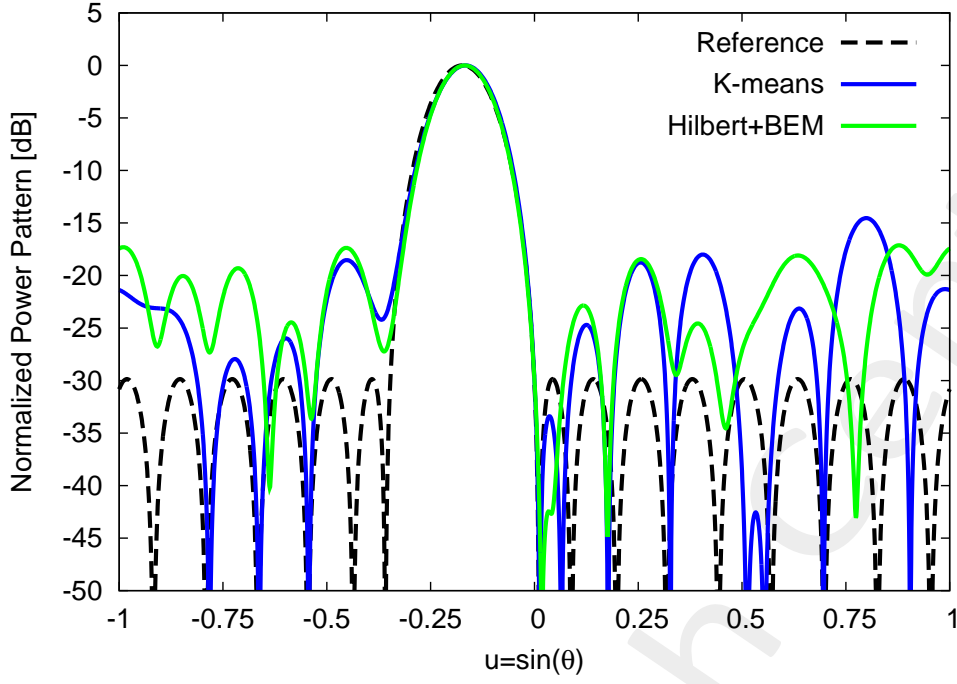
Figure 16: *Steered Pencil Beam* ($N = 16$, $Q = 8$, $\theta_0 = -10$ [deg]): power pattern of the clustered arrays synthetised with Hilbert+BEM, KMM together with the reference one.

| Ψ^{opt}	Φ^{opt}	Γ^{opt}	SLL [dB]	D [dBi]	$\Delta\tau$ [sec]
3.13×10^{-2}	6.33×10^{-2}	1.93×10^{-1}	-17.12	11.30	2.95×10^{-3}

Table X: *Steered Pencil Beam* ($N = 16$, $Q = 8$, $\theta_0 = -10$ [deg]): values of excitation matching index, Ψ^{opt}, the pattern matching index, Φ^{opt}, the pattern matching index Γ^{opt}, the SLL, the directivity D and the computational cost $\Delta\tau$.

	min	max	μ	σ^2
Ψ^{opt}	3.13×10^{-2}	6.78×10^{-2}	3.75×10^{-2}	4.59×10^{-6}
Φ^{opt}	6.33×10^{-2}	1.38×10^{-1}	7.68×10^{-2}	1.88×10^{-4}
SLL [dB]	-17.12	-12.93	-14.91	1.00
D [dBi]	11.00	11.35	11.25	11.02×10^{-2}

Table XI: Statistics (minimum value [min], maximum value [max], mean value [μ] and variance [σ^2]) calculated for the excitation matching Ψ^{opt}, the pattern matching index, Φ^{opt}, the SLL [dB] and the directivity D given $R = 50$ different random initialization.

Resume:

Hilbert Order	Ψ^{opt}	Φ^{opt}	Γ^{opt}	SLL [dB]	D [dBi]
$H = 1$	2.73×10^{-2}	5.51×10^{-2}	1.68×10^{-1}	-14.53	11.24
$H = 2$	3.10×10^{-2}	6.25×10^{-2}	1.92×10^{-1}	-16.30	11.30
$H = 3$	3.10×10^{-2}	6.26×10^{-2}	2.04×10^{-1}	-16.41	11.15
$H = 4$	3.24×10^{-2}	6.67×10^{-2}	1.87×10^{-1}	-15.78	11.15
$H = 5$	3.13×10^{-2}	6.33×10^{-2}	1.93×10^{-1}	-17.12	11.30
$H = 6$	3.24×10^{-2}	6.67×10^{-2}	1.87×10^{-1}	-15.78	11.15
$H = 7$	3.24×10^{-2}	6.67×10^{-2}	1.87×10^{-1}	-15.78	11.15
$H = 8$	3.24×10^{-2}	6.67×10^{-2}	1.87×10^{-1}	-15.78	11.15
$H = 9$	3.24×10^{-2}	6.67×10^{-2}	1.87×10^{-1}	-15.78	11.15
$H = 10$	3.13×10^{-2}	6.33×10^{-2}	1.93×10^{-1}	-17.12	11.30

Table XII: *Steered Pencil Beam* ($N = 16$, $Q = 8$, $\theta_0 = -10$ [deg]): values of the excitation matching index, Ψ^{opt}, the pattern matching index, Φ^{opt}, the pattern matching index Γ^{opt}, the SLL, the directivity D obtained for Hilbert curve Order $H = \{1, ..., 10\}$

Hilbert Order	Sorted Indexes															
$H = 1$	8	9	7	6	5	16	4	15	3	14	2	13	1	12	11	10
$H = 2$	8	9	7	6	5	4	16	15	2	14	3	13	12	1	10	11
$H = 3$	8	9	7	6	5	4	16	2	1	14	3	15	13	12	10	11
$H = 4$	8	9	7	6	5	4	16	1	2	14	3	15	13	12	10	11
$H = 5$	8	9	7	6	5	4	16	2	14	3	15	13	12	1	10	11
$H = 6$	8	9	7	6	5	4	16	1	2	14	3	15	13	12	10	11
$H = 7$	8	9	7	6	5	4	16	1	2	14	3	15	13	12	10	11
$H = 8$	8	9	7	6	5	4	16	1	2	14	3	15	13	12	10	11
$H = 9$	8	9	7	6	5	4	16	1	2	14	3	15	13	12	10	11
$H = 10$	8	9	7	6	5	4	16	2	14	3	15	13	12	1	10	11

Table XIII: *Steered Pencil Beam* ($N = 16$, $Q = 8$, $\theta_0 = -10$ [deg]): Hilbert excitations sorting vs Hilbert order

Observations:

- Increasing the Hilbert order H, some axial symmetries arise. For example, considering the first and second quadrant the imaginary axis becomes a line of symmetry, preventing the formation of suitable clusters during the optimization step, since some elements go away from each other.

- Sorting elements, according to the Hilbert Curve, some excitation near on the complex plane, are far along the curve. This happens in particular at the two endpoints of the curve. An explicative example is given by the excitations 9 and 10. Sorting the curve, starting from the left bottom edge and until the right bottom edge, the 9th excitation is always in the second position of the sorted list while the 10th element lies in the second to last ($H = \{2, ..., 10\}$) or last place ($H = 1$). Therefore, a possible suitable configuration will never take into account by this algorithm.

- From this first test case, it is emerged that after a certain Hilbert order H, the sorted list remained the same. Thus, in the following the analysis will be done taken into acocunt only the first 5 Hilbert curve orders.

Possible improvements:

- To reduce the excitations departure at curve endpoints, it can be useful to adopt, as sorting curve, a variant of the standard Hilbert curve, called *Moore Curve,* i.e. the loop version of the Hilbert curve. It may be thought as the union of four copies of the Hilbert curves combined in such a way to make the endpoints coincide.

- Moreover, it is also possible to develop a loop register version for the *Border Element Method* (BEM), allowing the formation of clusters from an endpoint to the other.

- Also the starting point of the sorting approach can cause a degradation or an improvement of the clustering property of the Border Element Method.

1.1.3 Effects of rotation on the Hilbert Curve Sorting

To understand the influence of the starting and end points of the Hilbert Curve on the sorting capabilities of the approach, let us change the starting point for the Hilber curve of order $H = 3$ and let us successively apply the Border Element Method.
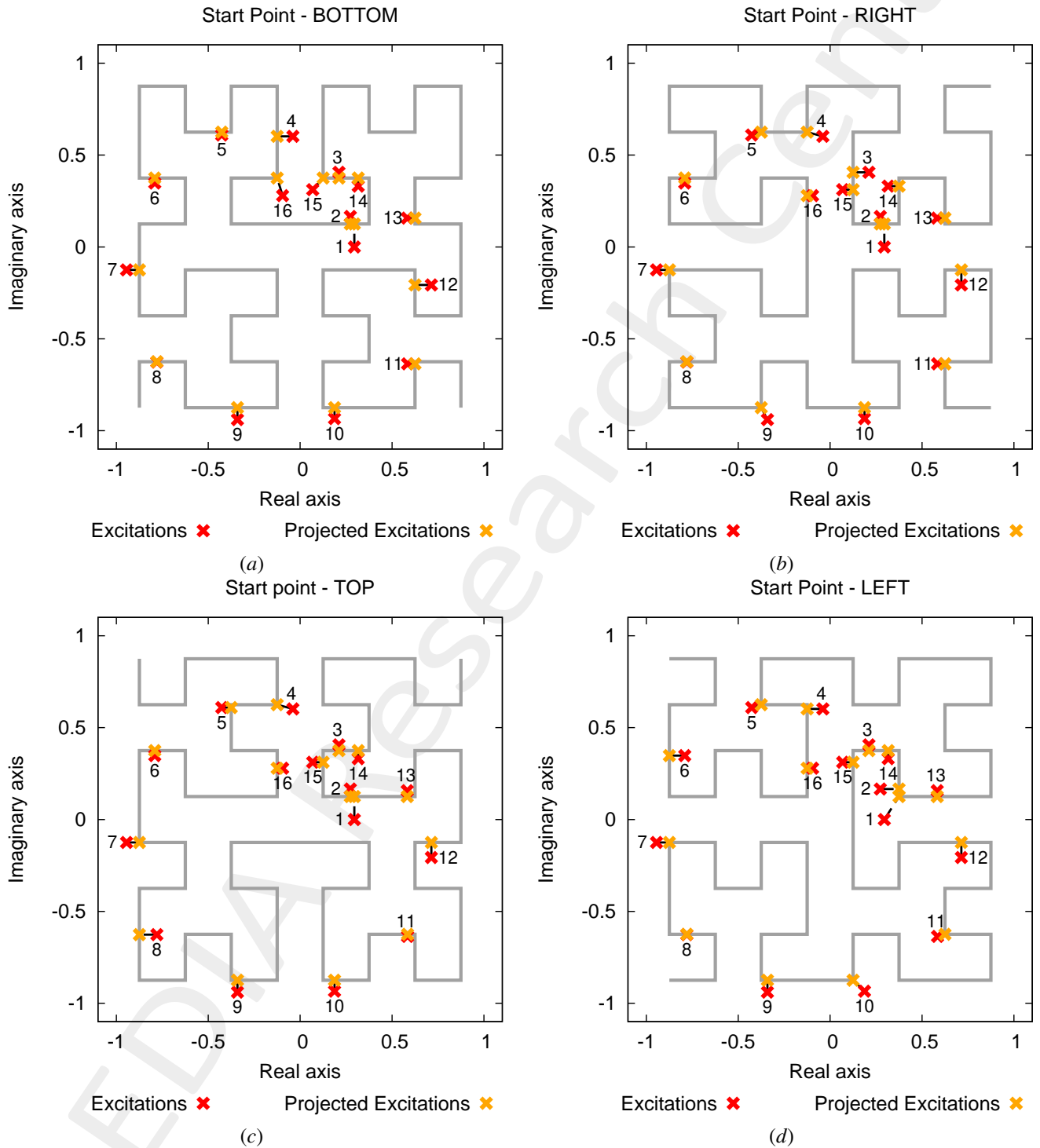

Figure 17: *Steered Pencil Beam* ($N = 16$, $Q = 8$, $\theta_0 = -10$ [deg]): Hilbert Curve Sorting varying the beginning point of the curve: (*a*) bottom, (*b*) right, (*c*) top and (*d*) left.

Starting point	Sorted Indexes															
BOTTOM	8	9	7	6	5	4	16	2	1	14	3	15	13	12	10	11
RIGHT	11	12	10	9	8	7	16	6	5	4	3	15	2	1	14	13
TOP	14	3	15	2	1	13	12	11	10	9	8	7	6	16	5	4
LEFT	6	16	4	5	13	1	2	14	3	15	12	11	10	9	7	8

Table XIV: *Steered Pencil Beam* ($N = 16$, $Q = 8$, $\theta_0 = -10$ [deg]): Hilbert excitations sorting vs starting curve point location.

Starting point	Excitations matching, Ψ^{opt}
BOTTOM	3.10×10^{-2}
RIGHT	3.33×10^{-2}
TOP	3.09×10^{-2}
LEFT	3.19×10^{-2}

Table XV: *Steered Pencil Beam* ($N = 16$, $Q = 8$, $\theta_0 = -10$ [deg]): excitation matching vs starting curve point location.

Observations:

- Even rotating the curve, the problem of sorting nearby points, sorted as far away from each other, persists. Thus, this problem is related with construction of the fractal curve itself. More in details, let us analyse the four cases:

    - the distance between the excitations number 9 and 10, which are in the extreme curve positions in the *BOTTOM* case, is lengthened in comparison with the other three cases (*RIGHT, TOP, LEFT*)

    - however, couples of excitations, which in principle are located near in the *BOTTOM* case, can become far for one of the other cases:

        * *LEFT:* excitations number 12 and 13

        * *TOP:* excitations number 6 and 7

        * *RIGHT:* excitations number $5 - 4 - 16$ and $3 - 14 - 15$

- Moreover, the excitations located in different quadrants, near in terms of distance, are sorted far away in all the cases. To better understand this concept, let us for example consider the excitation number $4 - 16$, in the second quadrant and $3 - 15$ in the first quadrant.

- Thus, the curve starting point partially affects the final subarray configuration. Every starting point has its own advantages and drawbacks, also related to the reference excitations distribution.

The Moore Curve, a loop version of the Hilbert curve, is in the following adopted for sorting the complex excitations. To compute the optimal subarray configuration the Border Element Method has been chosen. In the following the results obtained for order $H = 2, \ 3$ are reported.
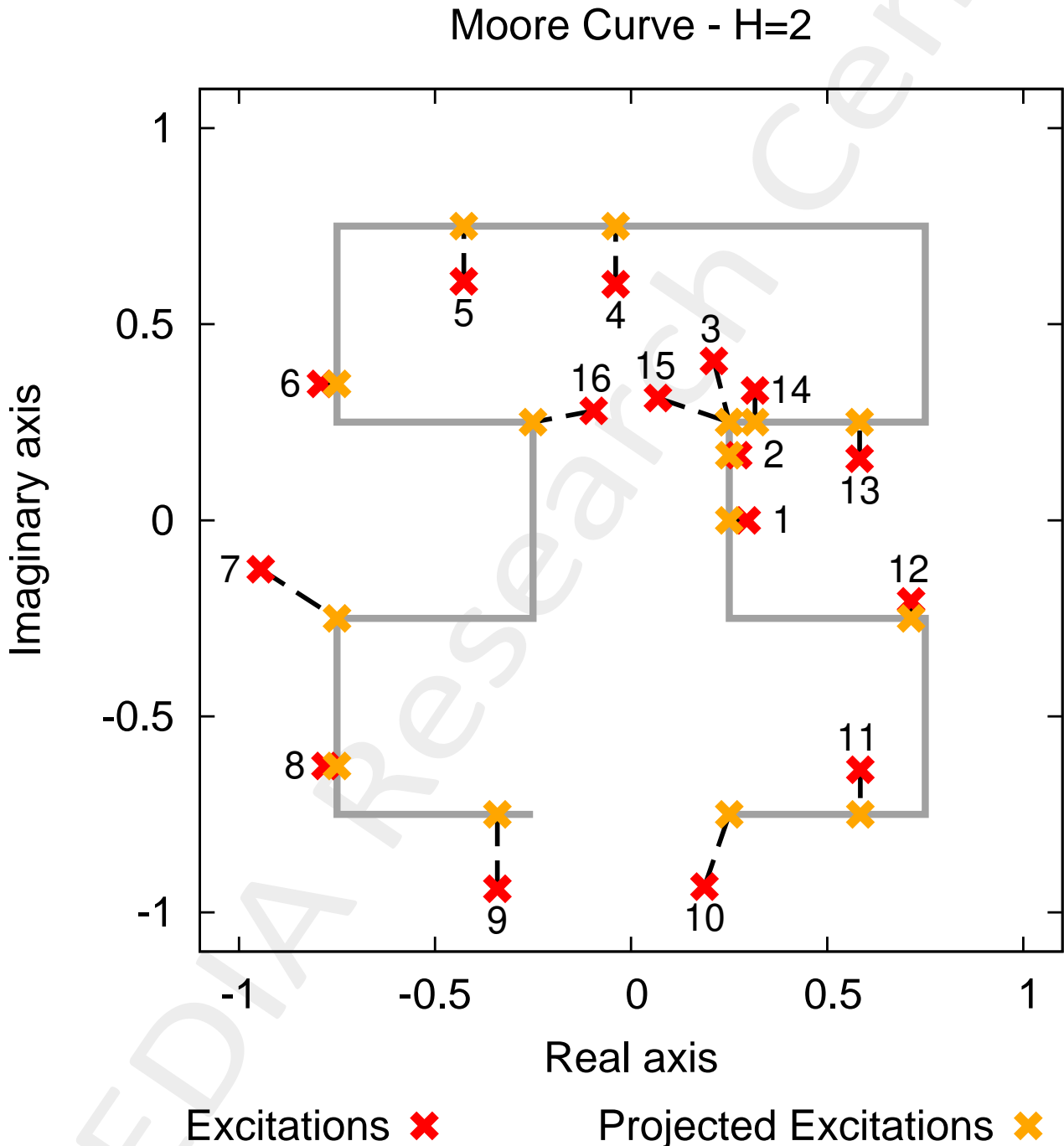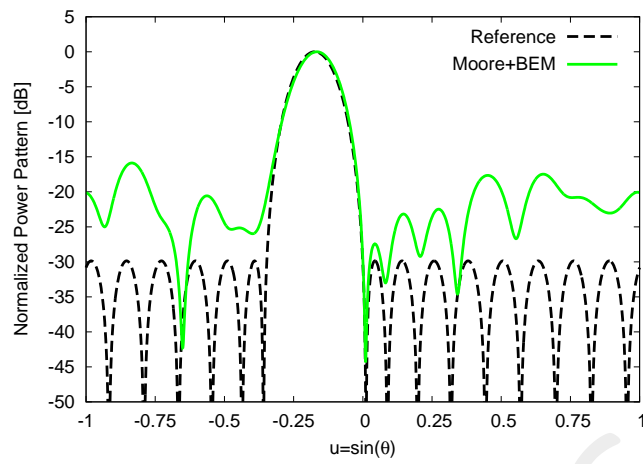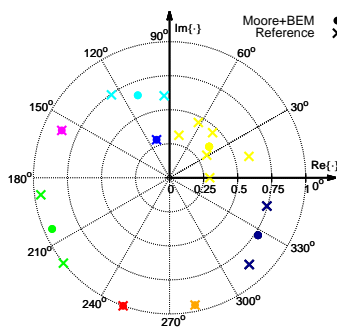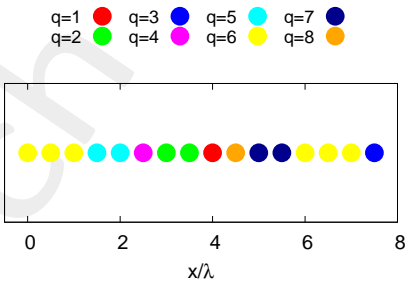
Moore Curve Order: H = 2

Figure 18: *Steered Pencil Beam* ($N = 16, Q = 8, \theta_0 = -10$ [deg]): projection of the 2D complex target excitations along the Moore Curve of order $H = 2$.

Figure 19: *Steered Pencil Beam* ($N = 16$, $Q = 8$, $\theta_0 = -10$ [deg]): plot of (*a*) the power pattern of the clusterized solutions together with the reference ones, (*b*) representation of the reference and the sub-array excitations in the complex plane, and (*c*) layout of the clustered array sythetized obtained with the best seed.
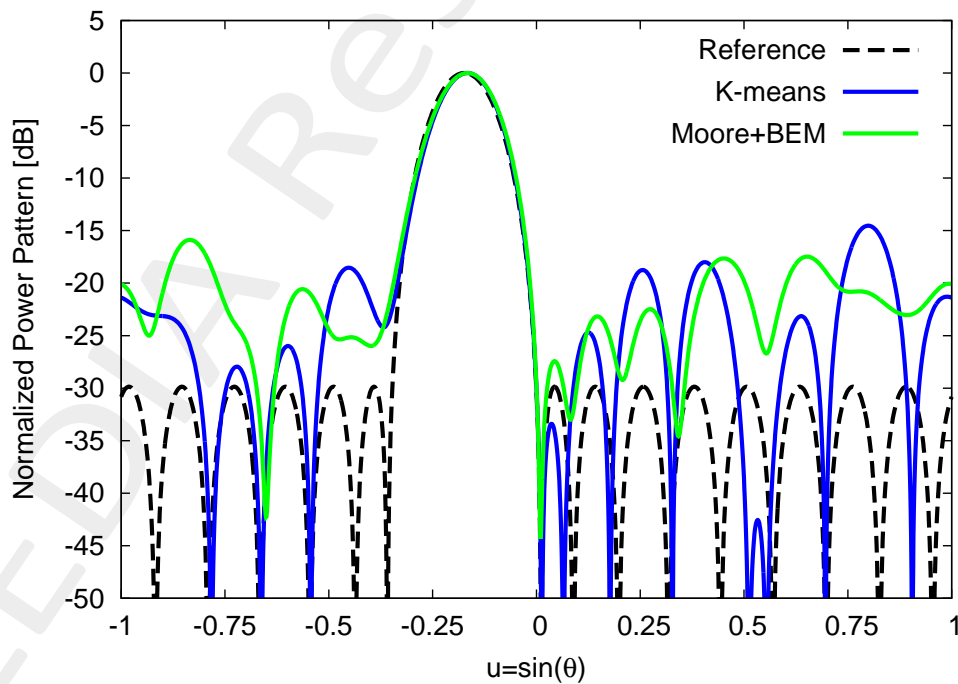

Figure 20: *Steered Pencil Beam* ($N = 16$, $Q = 8$, $\theta_0 = -10$ [deg]): power pattern of the clustered arrays synthetised with Moore+BEM, KMM together with the reference one.

Ψ^{opt}	Φ^{opt}	Γ^{opt}	SLL [dB]	D [dBi]	$\Delta\tau$ [sec]
3.54×10^{-2}	7.14×10^{-2}	2.06×10^{-1}	16.06	11.05	2.63×10^{-3}

Table XVI: *Steered Pencil Beam* ($N = 16$, $Q = 8$, $\theta_0 = -10$ [deg]): values of excitation matching index, Ψ^{opt}, the pattern matching index, Φ^{opt}, the pattern matching index Γ^{opt}, the SLL, the directivity D and the computational cost $\Delta\tau$, obtained with the standard BEM and the loop version of it.

	min	max	μ	σ^2
Ψ^{opt}	3.52×10^{-2}	6.99×10^{-2}	5.46×10^{-2}	1.03×10^{-4}
Φ^{opt}	7.14×10^{-2}	1.51×10^{-1}	1.11×10^{-1}	4.69×10^{-4}
SLL [dB]	-15.88	-11.98	-13.39	0.83
D [dBi]	10.85	11.16	11.05	4.32×10^{-3}

Table XVII: Statistics (minimum value [min], maximum value [max], mean value [μ] and variance [σ^2]) calculated for the excitation matching Ψ^{opt}, the pattern matching index, Φ^{opt}, the SLL [dB] and the directivity D given $R = 50$ different random initialization.

Figure 21: *Steered Pencil Beam* ($N = 16$, $Q = 8$, $\theta_0 = -10$ [deg]): projection of the 2D complex target excitations along the Moore Curve of order $H = 3$.

(a)
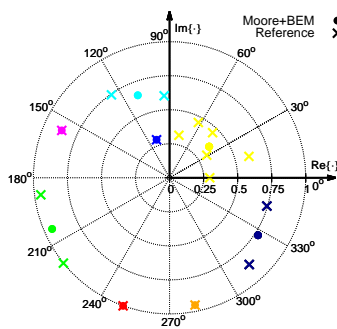
(b)
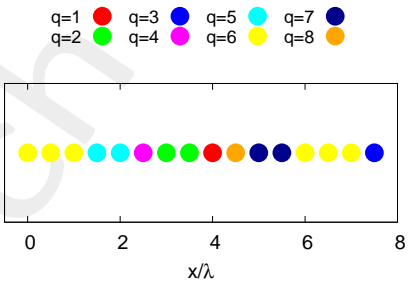
(c)

Figure 22: *Steered Pencil Beam* ($N = 16$, $Q = 8$, $\theta_0 = -10$ [deg]): plot of (*a*) the power pattern of the clusterized solutions together with the reference ones, (*b*) representation of the reference and the sub-array excitations in the complex plane, and (*c*) layout of the clustered array sythetized obtained with the best seed.
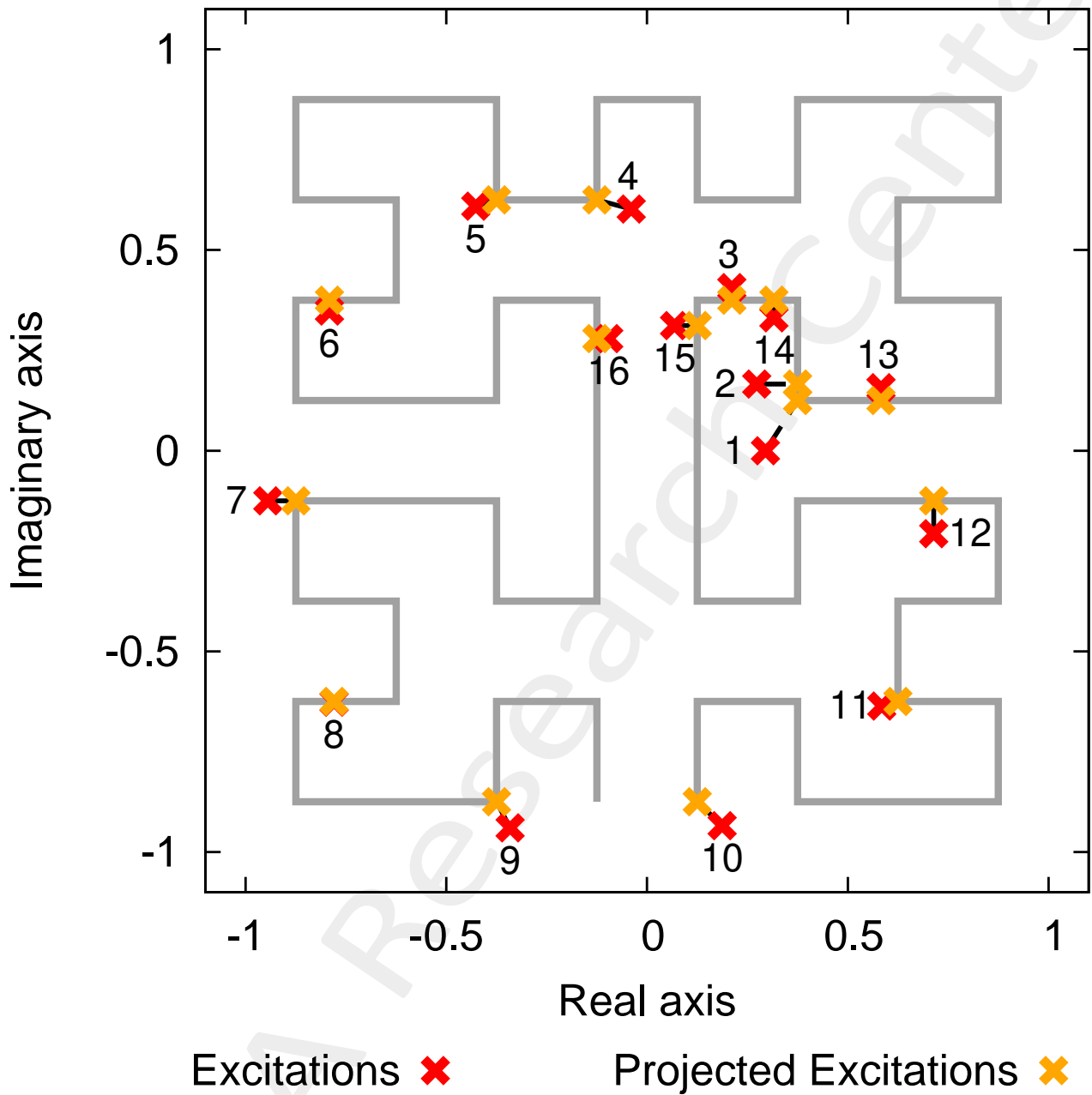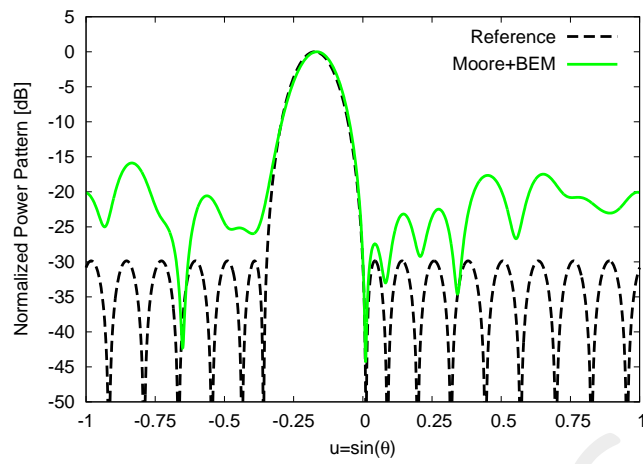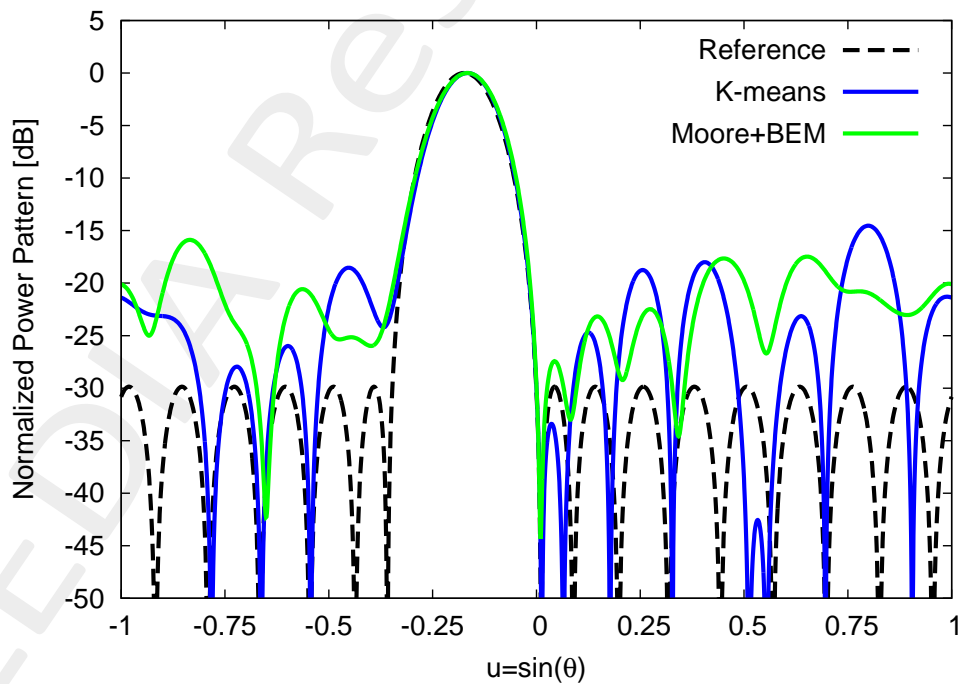

Figure 23: *Steered Pencil Beam* ($N = 16$, $Q = 8$, $\theta_0 = -10$ [deg]): power pattern of the clustered arrays synthetised with Moore+BEM, KMM together with the reference one.

Ψ^{opt}	Φ^{opt}	Γ^{opt}	SLL [dB]	D [dBi]	$\Delta\tau$ [sec]
3.54×10^{-2}	7.14×10^{-2}	2.06×10^{-1}	-16.06	11.05	2.16×10^{-2}

Table XVIII: *Steered Pencil Beam* ($N = 16$, $Q = 8$, $\theta_0 = -10$ [deg]): values of excitation matching index, Ψ^{opt}, the pattern matching index, Φ^{opt}, the SLL, the pattern matching index Γ^{opt}, the directivity D and the computational cost $\Delta\tau$, obtained with the standard BEM and the loop version of it.

	min	max	μ	σ^2
Ψ^{opt}	3.54×10^{-2}	8.83×10^{-2}	5.96×10^{-2}	1.54×10^{-4}
Φ^{opt}	7.14×10^{-2}	1.90×10^{-1}	1.24×10^{-1}	8.27×10^{-4}
SLL [dB]	-16.12	-11.64	-13.34	1.39
D [dBi]	10.95	11.28	11.10	6.64×10^{-3}

Table XIX: Statistics (minimum value [min], maximum value [max], mean value [μ] and variance [σ^2]) calculated for the excitation matching Ψ^{opt}, the pattern matching index, Φ^{opt}, the SLL [dB] and the directivity D given $R = 50$ different random initialization.

Resume:

| Hilbert Order	Ψ^{opt}	Φ^{opt}	Γ^{opt}	SLL [dB]	D [dBi]
$H = 1$	2.73×10^{-2}	5.51×10^{-2}	1.68×10^{-1}	-14.53	11.24
$H = 2$	3.54×10^{-2}	7.14×10^{-2}	2.06×10^{-1}	16.06	11.05
$H = 3$	3.54×10^{-2}	7.14×10^{-2}	2.06×10^{-1}	16.06	11.05
$H = 4$	3.54×10^{-2}	7.14×10^{-2}	2.06×10^{-1}	16.06	11.05
$H = 5$	3.54×10^{-2}	7.14×10^{-2}	2.06×10^{-1}	16.06	11.05

Table XX: *Steered Pencil Beam* ($N = 16$, $Q = 8$, $\theta_0 = -10$ [deg]): values of the excitation matching index, Ψ^{opt}, the pattern matching index, Φ^{opt}, the pattern matching index Γ^{opt}, the SLL, the directivity D obtained for Hilbert curve Order $H = \{1, ..., 10\}$

Hilbert Order	Sorted Indexes															
$H = 1$	8	9	7	6	5	16	4	15	3	14	2	13	1	12	11	10
$H = 2$	9	8	7	16	6	5	4	13	14	3	15	2	1	12	11	10
$H = 3$	9	8	7	16	6	5	4	13	1	2	14	3	15	12	11	10
$H = 4$	9	8	7	16	6	5	4	13	1	2	14	3	15	12	11	10
$H = 5$	9	8	7	16	6	5	4	13	1	2	14	3	15	12	11	10

Table XXI: *Steered Pencil Beam* ($N = 16$, $Q = 8$, $\theta_0 = -10$ [deg]): Hilbert excitations sorting vs Hilbert order

Observations:

For this test case the Moore Curve sorting performs worst compared with the the Hilbert Curve sorting. Nevertheless, in some cases it can be useful to test also this sorting approach.

In order to overcome the limitations of space-filling curve sorting algorithm, let us analyse the performance of the Spectral LPM Sorting.

Figure 24: *Steered Pencil Beam* ($N = 16$, $Q = 8$, $\theta_0 = -10$ [deg]): complex target excitations sorted according to the Spectral LPM algorithm.
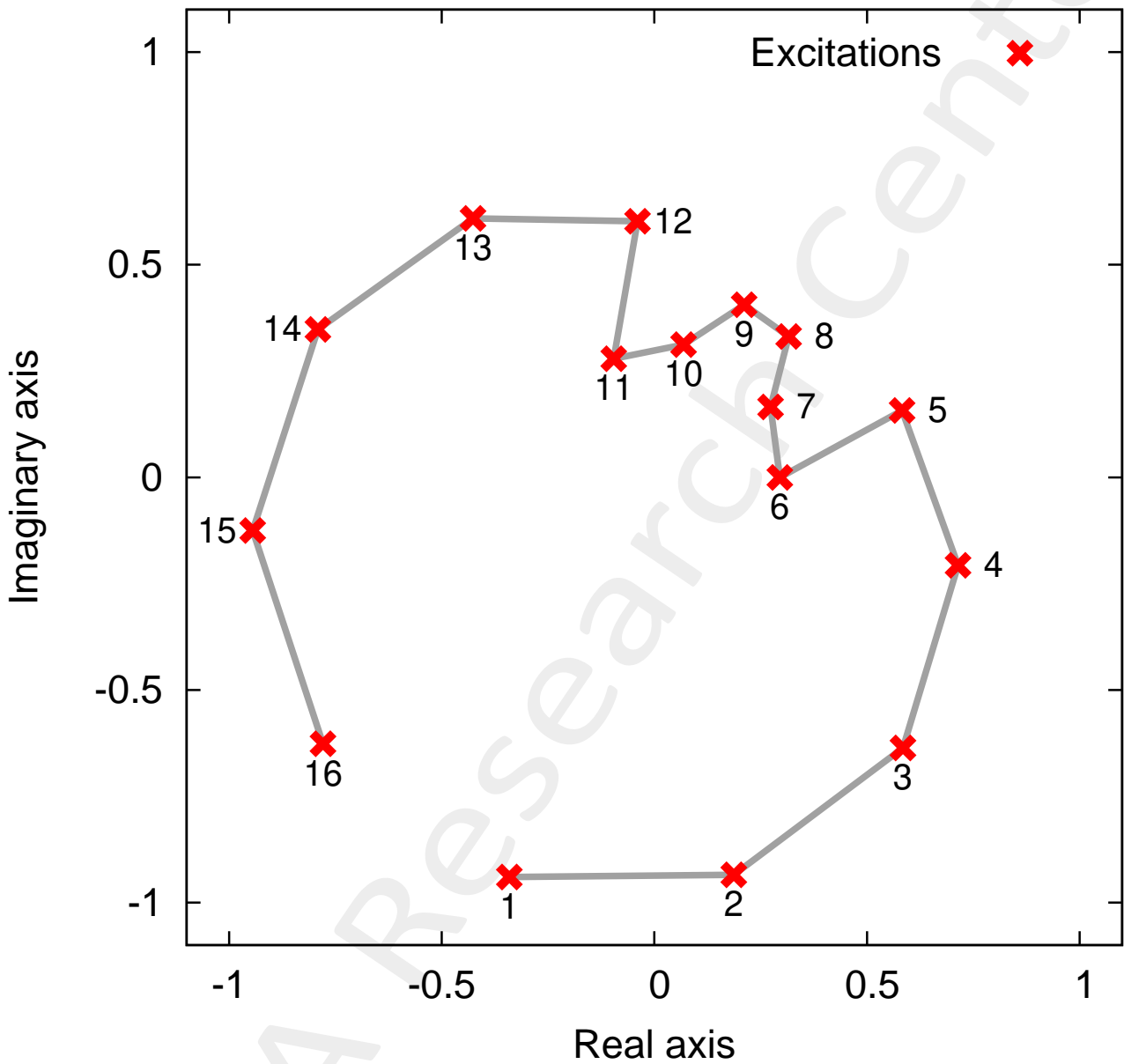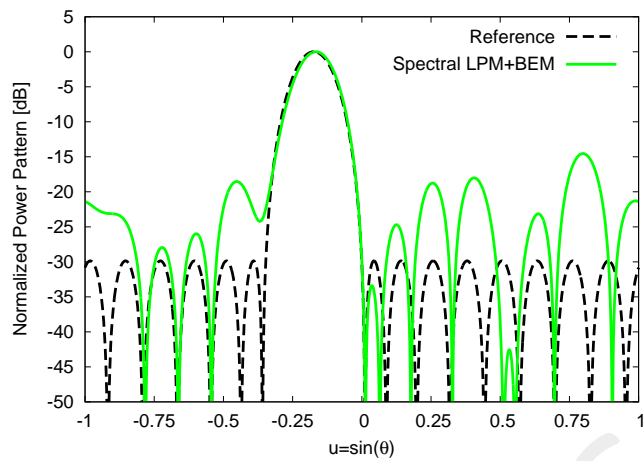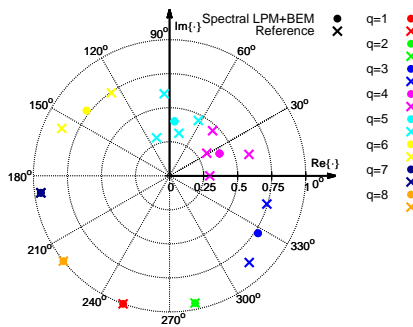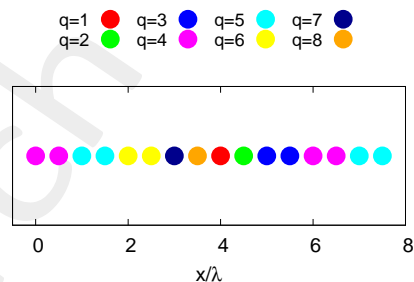
Figure 25: *Steered Pencil Beam* ($N = 16$, $Q = 8$, $\theta_0 = -10$ [deg]): plot of (*a*) the power pattern of the clusterized solutions together with the reference ones, (*b*) representation of the reference and the sub-array excitations in the complex plane, and (*c*) layout of the clustered array sythetized with *Spectral LPM+BEM*, obtained with the best seed.
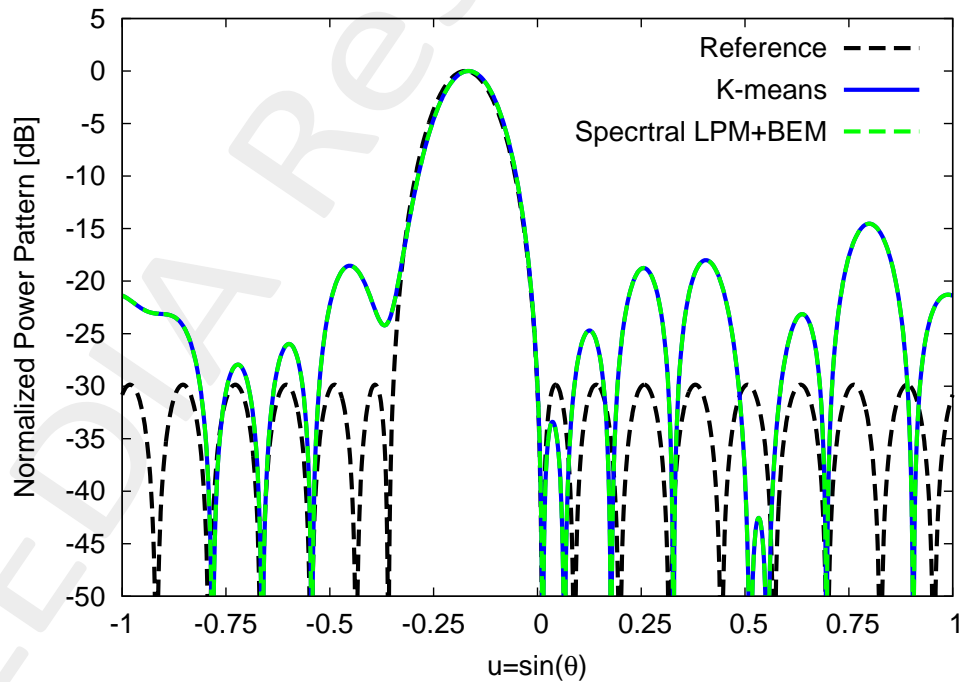

Figure 26: *Steered Pencil Beam* ($N = 16$, $Q = 8$, $\theta_0 = -10$ [deg]): power pattern of the clustered arrays synthetised with Spectral LPM+BEM, KMM together with the reference one.

Ψ^{opt}	Φ^{opt}	Γ^{opt}	SLL [dB]	D [dBi]	$\Delta\tau$ [sec]
2.73×10^{-2}	5.51×10^{-2}	1.68×10^{-1}	-14.53	11.24	0.00

Table XXII: *Steered Pencil Beam* ($N = 16$, $Q = 8$, $\theta_0 = -10$ [deg]): values of excitation matching index, Ψ^{opt}, the pattern matching index, Φ^{opt}, the pattern matching index Γ^{opt}, the SLL, the directivity D and the computational cost $\Delta\tau$.

	min	max	μ	σ^2
Ψ^{opt}	2.73×10^{-2}	3.14×10^{-2}	3.00×10^{-2}	2.41×10^{-6}
Φ^{opt}	5.51×10^{-2}	6.34×10^{-2}	6.06×10^{-2}	9.59×10^{-6}
SLL [dB]	-15.83	-13.68	-14.06	0.17
D [dBi]	11.16	11.26	11.25	2.63×10^{-4}

Table XXIII: Statistics (minimum value [min], maximum value [max], mean value [μ] and variance [σ^2]) calculated for the excitation matching Ψ^{opt}, the pattern matching index, Φ^{opt}, the SLL [dB] and the directivity D given $R = 50$ different random initialization.

Observation:

From an initial analysis, the Spectral LPM algorithm seems to sort well the complex array excitations, however a deeper understanding of the method performace is necessary.

More information on the topics of this document can be found in the following list of references.

References

[1] N. Anselmi, L. Tosi, P. Rocca, G. Toso, and A. Massa, "A self-replicating single-shape tiling technique for the design of highly modular planar phased arrays - The case of L-shaped rep-tiles," *IEEE Trans. Antennas Propag.* , vol. 71, no. 4, pp. 3335-3348, Apr. 2023.

[2] A. Benoni, P. Rocca, N. Anselmi, and A. Massa, "Hilbert-ordering based clustering of complex-excitations linear arrays," *IEEE Trans. Antennas Propag.* , vol. 70, no. 8, pp. 6751-6762, Aug. 2022.

[3] P. Rocca, L. Poli, N. Anselmi, and A. Massa, "Nested optimization for the synthesis of asymmetric shaped beam patterns in sub-arrayed linear antenna arrays," *IEEE Trans. Antennas Propag.* , vol. 70, no. 5, pp. 3385 - 3397, May 2022.

[4] P. Rocca, L. Poli, A. Polo, and A. Massa, "Optimal excitation matching strategy for sub-arrayed phased linear arrays generating arbitrary shaped beams," *IEEE Trans. Antennas Propag.*, vol. 68, no. 6, pp. 4638-4647, Jun. 2020.

[5] G. Oliveri, G. Gottardi and A. Massa, "A new meta-paradigm for the synthesis of antenna arrays for future wireless communications," *IEEE Trans. Antennas Propag.*, vol. 67, no. 6, pp. 3774-3788, Jun. 2019.

[6] P. Rocca, M. H. Hannan, L. Poli, N. Anselmi, and A. Massa, "Optimal phase-matching strategy for beam scanning of sub-arrayed phased arrays," *IEEE Trans. Antennas and Propag.*, vol. 67, no. 2, pp. 951-959, Feb. 2019.

[7] N. Anselmi, P. Rocca, M. Salucci, and A. Massa, "Contiguous phase-clustering in multibeam-on-receive scanning arrays," IEEE Trans. *Antennas Propag.*, vol. 66, no. 11, pp. 5879-5891, Nov. 2018.

[8] L. Poli, G. Oliveri, P. Rocca, M. Salucci, and A. Massa, "Long-Distance WPT Unconventional Arrays Synthesis," *J. Electromagn. Waves Appl. J.*, vol. 31, no. 14, pp. 1399-1420, Jul. 2017.

[9] G. Gottardi, L. Poli, P. Rocca, A. Montanari, A. Aprile, and A. Massa, "Optimal Monopulse Beamforming for Side-Looking Airborne Radars," *IEEE Antennas Wireless Propag. Lett.*, vol. 16, pp. 1221-1224, 2017.

[10] G. Oliveri, M. Salucci, and A. Massa, "Synthesis of modular contiguously clustered linear arrays through a sparseness-regularized solver," *IEEE Trans. Antennas Propag.*, vol. 64, no. 10, pp. 4277-4287, Oct. 2016.

[11] P. Rocca, G. Oliveri, R. J. Mailloux, and A. Massa, "Unconventional phased array architectures and design Methodologies - A review," *Proc. IEEE*, Invited Paper, vol. 104, no. 3, pp. 544-560, March 2016.

[12] P. Rocca, M. D'Urso, and L. Poli, "Advanced strategy for large antenna array design with subarray-only amplitude and phase control," *IEEE Antennas and Wireless Propag. Lett.*, vol. 13, pp. 91-94, 2014.

[13] L. Manica, P. Rocca, G. Oliveri, and A. Massa, "Synthesis of multi-beam sub-arrayed antennas through an excitation matching strategy," *IEEE Trans. Antennas Propag.*, vol. 59, no. 2, pp. 482-492, Feb. 2011.

[14] G. Oliveri, "Multi-beam antenna arrays with common sub-array layouts," *IEEE Antennas Wireless Propag. Lett.*, vol. 9, pp. 1190-1193, 2010.

[15] P. Rocca, R. Haupt, and A. Massa, "Sidelobe reduction through element phase control in sub-arrayed array antennas," *IEEE Antennas Wireless Propag. Lett.*, vol. 8, pp. 437-440, 2009.

[16] P. Rocca, L. Manica, R. Azaro, and A. Massa, "A hybrid approach for the synthesis of sub-arrayed monopulse linear arrays," *IEEE Trans. Antennas Propag.* , vol. 57, no. 1, pp. 280-283, Jan. 2009.

[17] L. Manica, P. Rocca, M. Benedetti, and A. Massa, "A fast graph-searching algorithm enabling the efficient synthesis of sub-arrayed planar monopulse antennas," *IEEE Trans. Antennas Propag.*, vol. 57, no. 3, pp. 652-664, Mar. 2009.

[18] P. Rocca, L. Manica, A. Martini, and A. Massa, "Compromise sum-difference optimization through the iterative contiguous partition method," *IET Microwaves, Antennas & Propagation*, vol. 3, no. 2, pp. 348-361, 2009.

[19] L. Manica, P. Rocca, and A. Massa, "An excitation matching procedure for sub-arrayed monopulse arrays with maximum directivity," *IET Radar, Sonar & Navigation*, vol. 3, no. 1, pp. 42-48, Feb. 2009.

[20] L. Manica, P. Rocca, and A. Massa, "Design of subarrayed linear and planar array antennas with SLL control based on an excitation matching approach," *IEEE Trans. Antennas Propag.*, vol. 57, no. 6, pp. 1684-1691, Jun. 2009.

[21] L. Manica, P. Rocca, A. Martini, and A. Massa, "An innovative approach based on a tree-searching algorithm for the optimal matching of independently optimum sum and difference excitations," *IEEE Trans. Antennas Propag.*, vol. 56, no. 1, pp. 58-66, Jan. 2008.

[22] P. Rocca, L. Manica, and A. Massa, "An effective excitation matching method for the synthesis of optimal compromises between sum and difference patterns in planar arrays," *Progress in Electromagnetic Research B*, vol. 3, pp. 115-130, 2008.

[23] P. Rocca, L. Manica, and A. Massa, "Directivity optimization in planar sub-arrayed monopulse antenna," *Progress in Electromagnetic Research L*, vol. 4, pp. 1-7, 2008.

[24] P. Rocca, L. Manica, M. Pastorino, and A. Massa, "Boresight slope optimization of sub-arrayed linear arrays through the contiguous partition method," *IEEE Antennas Wireless Propag. Lett.*, vol. 8, pp. 253-257, 2008.

[25] P. Rocca, L. Manica, and A. Massa, "Synthesis of monopulse antennas through the iterative contiguous partition method," *Electronics Letters*, vol. 43, no. 16, pp. 854-856, Aug. 2007.

[26] P. Rocca, L. Manica, A. Martini, and A. Massa, "Synthesis of large monopulse linear arrays through a tree-based optimal excitations matching," *IEEE Antennas Wireless Propag. Lett.*, vol. 7, pp. 436-439, 2007.